IDŐJÁRÁS

QUARTERLY JOURNAL
OF THE HUNGARIAN METEOROLOGICAL SERVICE

CONTENTS

****

http://www.met.hu/Journal-Idojaras.php

VOL. 114 * NO. 3 * JULY – SEPTEMBER 2010

IDŐJÁRÁS

Quarterly Journal of the Hungarian Meteorological Service

Editorial Office: Gilice tér 39, H-1182 Budapest, Hungary
P.O. Box 39, H-1675 Budapest, Hungary
E-mail: bozo.l@met.hu or antal.e@met.hu
Fax: (36-1) 346-4809

Indexed and abstracted in Science Citation Index Expanded™ and Journal Citation Reports/Science Edition
Covered in the abstract and citation database SCOPUS®

Subscription by

mail: IDŐJÁRÁS, P.O. Box 39, H-1675 Budapest, Hungary
E-mail: kenderesy.k@met.hu or antal.e@met.hu

IDŐJÁRÁS

Quarterly Journal of the Hungarian Meteorological Service
Vol. 114, No. 3, July–September 2010, pp. 153–168

Neural networks for precipitation forecasting in Bulgaria

Ivan V. Tsonevsky* and **Valery G. Spiridonov**

National Institute of Meteorology and Hydrology
66 Tsarigradsko Chaussee, Sofia 1784, Bulgaria; E-mail: Ivan.Tzonevski@meteo.bg

**Corresponding author*

(Manuscript received in final form October 15, 2009)

Abstract—The application of neural networks for forecasting precipitation in Bulgaria is discussed in this note. The problem is to determine whether a given forecasted precipitation event would exceed the operational criteria for a heavy-snow warning in the cool season (October–March) or a heavy-rain warning in the warm season (April–September) (10 mm and 15 mm in 12 hours, respectively). The inputs to two sets of four multilayer perceptrons (MLPs) were selected from among 27 variables extracted from the global numerical weather prediction model from the UK Met Office. These variables (e.g., 850 hPa and 500 hPa temperatures and wind) were picked, because they are more predictable than the amount of precipitation. Bulgaria was divided into six geographic regions, and all MLPs were trained independently for each region. The training dataset consisted of all 12-hour periods with precipitation of the years 1998–2004. The MLPs performed better during the cool season; the mean of the correct classifications across all regions was 75% in the cool season and 65% in the warm season. Sensitivity analysis enabled a determination of the relative importance of each of the 27 variables to the performance of the neural network. The most important variables were temperature and wind fields at both 850 and 500 hPa levels. A combined system of MLPs ensemble and operational limited area numerical weather prediction model ALADIN is presented that shows better skill in forecasting heavy precipitation events.

Key-words: artificial neural networks, weather forecasting, heavy precipitation, NWP models, weather warnings

1. Introduction

Numerical weather prediction (NWP) models have improved considerably during the last few decades. For example, the European Centre for Medium-Range Weather Forecasts model showed gains of one day in predictability of mean sea level pressure and 500 hPa height over the last decade of the twentieth century in the Northern Hemisphere (*Simmons* and *Hollingsworth*, 2002).

Precipitation forecasts showed the same improvement over Europe (*Ghelli*, 2006). Because precipitation has an inherently small spatial scale and low predictability (*Rodwell*, 2006), precipitation events exceeding 60 mm/day are poorly represented by NWP models (e.g., *Lalaurette* and *van der Grijn*, 2006). Many statistical methods can be used to improve the raw output of NWP models such as model output statistics (MOS; *Glahn* and *Lowry*, 1972) and downscaling (*Wilby* and *Wigley*, 1997).

Another way to improve precipitation forecasts is using artificial neural networks (ANN). Neural networks have been applied in meteorology for classification and prediction by many authors (e.g., *Banket*, 1994; *Xiao* and *Chandrasekar*, 1997; *Hall et al.*, 1999; *Marzban*, 2000; *Chevallier et al.*, 2000; *Zhanqing et al.*, 2001; *Roebber et al.*, 2003).

The purpose of our investigation is to develop a tool for forecasting of heavy precipitation events in Bulgaria over six different geographically distinct regions. NWP models explicitly predict the variables included in the model equations, more accurately than the precipitation. On the other hand, experienced forecasters can draw upon pattern recognition to skilfully predict dry and wet situations. We used some of the most predictable variables to train a number of neural networks specifying the regions with heavy precipitation.

The main objective of this investigation is to find an appropriate modern tool, such as neural networks, for applying the classical synoptic rules for improving NWP forecast of heavy precipitation. Hence, our goal is to give forecasters additional information to the available operational NWP predictions (deterministic and probabilistic) in order to increase their confidence treating heavy precipitation situations.

In Section 2, the datasets used to train the neural networks are described. In Section 3, the structure of two sets of four multilayer perceptrons (MLPs) are presented and tested on precipitation data of the years 1998–2004. In Section 4, ALADIN NWP model predictions and those of a combined system (ALADIN+ANN ensemble) are compared using a dataset of precipitation events from 2005, and Section 5 concludes this paper.

2. Data

Neural networks have to learn the input–output relationship through a training process. In supervised learning, the training dataset contains examples of inputs with corresponding outputs. We chose the input variables from archived analysis of the Met Office's global NWP model in GRID code with spatial resolution of 2.5° latitude × 2.5° longitude at three levels: surface, 850 hPa, and 500 hPa. The following 27 variables served as inputs to the neural networks: latitude and longitude of the centers of the closest cyclone and anticyclone at each level to Bulgaria (12 variables in total); mean sea level pressure and geopotential heights at 850 and 500 hPa of these centers (6 variables); wind speed and wind direction

at 850 and 500 hPa at the model grid point closest to the geographic region in Bulgaria (4 variables); temperatures at 850 and 500 hPa, as well as the difference between these temperatures ($\Delta T_1 = T_{850}(\varphi_r,\lambda_r) - T_{500}(\varphi_r,\lambda_r)$) at the same grid point with geographical coordinates (φ_r,λ_r); and two horizontal temperature differences at 850 hPa over Bulgaria: $\Delta T_2 = T_{850}(\varphi_1,\lambda_1) - T_{850}(\varphi_2,\lambda_2)$ and $\Delta T_3 = T_{850}(\varphi_3,\lambda_3) - T_{850}(\varphi_4,\lambda_4)$, where φ_1= 45.0° N, λ_1= 30.0° E, φ_2= 42.5° N, λ_2= 22.5° E, φ_3= 45.0° N, λ_3= 20,0° E, φ_4= 42.5° N, λ_4= 27.5° E are the geographical coordinates of the grid points. The horizontal temperature differences at 850 hPa are a measure of the presence of frontal zones and represent the dominant directions of the movement of the fronts over Bulgaria (ΔT_2 and ΔT_3 represent the northeast–southwest and northwest–southeast directions, respectively). Our choices of input variables were based on the following two criteria: their availability in the archive and their predictability. The selected variables are much more predictable than the precipitation, thus serving to represent the large-scale pattern. We tried to use the most predictable, dynamic variables which allow us to extend the neural network approach beyond the first 12 hours even in the medium range keeping high confidence of the forecasts. Here, the neural network technique could be considered as the development of the classical synoptic method, which uses the evolution of the weather systems (such as cyclones and anticyclones) to predict the precipitation over some region not including explicitly the humidity. The reason is that the humidity in NWP models depends on the fluxes from the surface and the evaporation of precipitation. These processes are parameterized and hence the humidity is less predictable than the temperature, geopotential, or mean sea-level pressure, which are product of the physical equations in the dynamical component of the model. On the other hand, since the humidity or precipitable water and the precipitation amounts are very closely connected, we may expect that adding the humidity as an input would dominate the other more predictable variables such as geopotential and temperature. Therefore, neural networks are not used here for statistical post-processing of NWP model's output but are used as a model that include classical synoptic rules which, in combination with NWP model, gives better results.

The difference ΔT_1 between temperatures at 850 and 500 hPa is a measure of atmospheric stability, included in all neural networks in the warm season when convection is a dominant precipitation mechanism. In future investigations, the influence of other measures of stability, such as convective available potential energy (CAPE) and lifted index, could be examined.

The centers of cyclones and anticyclones are determined automatically and if there is not any close circulation system, the minimum and, respectively, the maximum value over the boundaries of the European region and their geographical coordinates are taken as inputs. We calculate the distance between the closest circulation centers and a point situated at the center of Bulgaria.

The output variable is the precipitation class, indicating whether the precipitation amount for the 12-hour period exceeded a given seasonal threshold. The precipitation class is a nominal variable that has two values: '0' if the precipitation amount is below the threshold and '1' if the precipitation amount is above this threshold. Since the dominant precipitation mechanism in the cool season is generally different than that in summer, we created two training sets with two different thresholds. In the warm season (April–September), when convective precipitation dominates, we chose the threshold to be 15 mm/12 hours, consistently with the operational criterion for heavy-rain warning in Bulgaria. Similarly, in the cool season (October–March), stratiform precipitation dominates and usually falls as snow. Therefore, we chose the threshold to be 10 mm/12 hours, or about 10 cm snow/12 hours, which is the operational criterion for heavy-snow warning in Bulgaria.

The design of the neural network suggests that a relationship exists between the inputs chosen above and the output precipitation class. In practice, however, we do not know the exact relationship between the inputs and output. The training datasets contain all the cases of the years 1998–2004 when precipitation was measured; hence they are representative and balanced datasets. This means that the proportion of the different classes in the dataset is the same as it was measured, which is of critical importance to the training. Precipitation amounts are taken from the daily standard observations from the network of 34 synoptic stations over Bulgaria (*Fig. 1*). In order to obtain the nominal output (i.e., the precipitation class), the maximum precipitation amount for each region is selected.

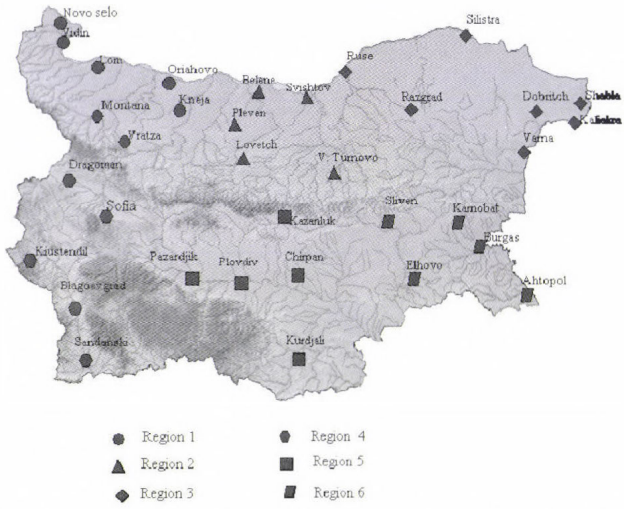

Fig. 1. Distribution of the synoptic stations over the territory of Bulgaria used for dataset construction (different marks of the stations represent their belonging to different regions).

3. Construction and training of the neural network sets

Classification can be performed using a wide range of neural network types. We used the multilayer perceptron (MLP), because this is perhaps the most popular network architecture in use today, providing wide applicability and ability to model very complex nonlinear functions. Moreover, MLP can be trained by various training algorithms such as the back propagation (e.g., *Werbos*, 1974; *Parker*, 1985; *Rumelhart et al.*, 1986), conjugate gradient descent (e.g., *Bishop*, 1995; *Shepherd*, 1997), and Levenberg–Marquardt algorithms (*Levenberg*, 1944; *Marquardt*, 1963). We used the first two algorithms in our training procedure. MLP has a simple interpretation as an input-output model with one or more hidden layers, each of them consists of a number of hidden units. A network with a single hidden layer is in practice capable of modeling most real classification problems.

The first step in constructing the MLPs was to divide Bulgaria into an appropriate number of regions. Taking into account the orography and some geographical features, we divided Bulgaria into six regions (*Fig. 1*):

Region 1 = northwestern part of Bulgaria,
Region 2 = central part of northern Bulgaria,
Region 3 = northeastern part of Bulgaria,
Region 4 = southwestern part of Bulgaria containing Sofia, the capital of the country,
Region 5 = central part of southern Bulgaria,
Region 6 = southeastern part of Bulgaria.

To design MLPs, we used STATISTICA Neural Networks, a software package for neural-network applications. Using the options in STATISTICA Neural Networks, we randomly divided each dataset into three sections necessary for the training process: a training set, a verification set, and a test set. The verification set is used to track the network's error performance, to identify the best network, and to stop training if over-learning occurs. The test set is not used in training at all, and is designed to give an independent assessment of the network's performance when an entire network design procedure is completed. We selected initial configurations of MLPs by choosing one hidden layer, because experiments with two and more hidden layers did not lead to better performance of the networks. Conducting sensitivity analysis, we selected three configurations with different input variables for each season and region. Sensitivity analysis, discussed in more detail in Section 3.3, rates the importance of variables. Then, we conducted a large number of experiments with different configurations with a different number of hidden units to obtain the network with the lowest verification error. Determining the hidden units is important, but not easy. If the number of the hidden units is too large, overfitting may occur, and the verification error rises while the training error decreases. In this context,

we performed a huge number of experiments to determine the number of hidden units starting with a half of the number of input units. Varying the number of hidden units helped to choose the neural network with the best performance. Following the training process, each network was run on the independent test dataset that is not used in the training, giving an independent assessment of the networks' performance. The activation function of the hidden and output layers is the logistic function. The latter guarantees an output lying in the range (0, 1). The target output '1' indicates membership in one class and '0' represents membership in the other. The error function used in the training is very important (*Bishop*, 1995). We used sum-squared error function appropriate for classification.

The selected configurations were trained many times to avoid local minima. The configuration with all 27 input variables was also trained. This training process was repeated for each region independently. Finally, for each region, the result was two neural network sets (cool and warm season) consisting of four MLPs. These networks are combined into an ensemble.

3.1. Neural network set for the cool season

(a) MLP (7, 8)

The first MLP from the cool-season network set consists of 7 input variables and 8 hidden units: MLP (7, 8). The input variables are: latitude and longitude of the centers of the closest cyclone to Bulgaria at 850 hPa; wind speed and wind direction at 500 hPa at the model grid point closest to the examined region; temperature at 850 hPa and vertical temperature difference (ΔT_1) at the same grid point; temperature difference in the northwest-southeast direction (ΔT_2).

(b) MLP (8, 11)

The second MLP has 8 inputs and 11 hidden units. The input variables are: latitude and longitude of the centers of the closest cyclone to Bulgaria at 850 hPa; wind speed and wind direction at 500 hPa at the model grid point closest to the examined region; temperature differences at 850 hPa in the northeast-southwest and northwest-southeast directions (ΔT_2 and ΔT_3, respectively); wind speed and wind direction at 850 hPa at the model grid point closest to the examined region.

(c) MLP (5, 16)

The third MLP of the ensemble has 5 inputs and 16 hidden units. The input variables are: wind speed and wind direction at 500 hPa in the model grid point closest to the examined region; vertical temperature gradient ΔT_1 in the same grid point; temperature differences ΔT_2 and ΔT_3 at 850 hPa in northeast-southwest and northwest-southeast direction, respectively.

(d) MLP (27, 14)

The last MLP from the ensemble contains all 27 variables described in Section 2 and has 14 hidden units.

The performance is a measure of the success of the network and gives the percentage of cases correctly classified. The performance of the neural networks during the cool season varies from region to region. The mean for all regions is 70%.

3.2. Neural network set for the warm season

There is also a set of four MLPs for the warm season.

(a) MLP (4, 14)

The first neural network is an MLP with 4 inputs and 14 hidden units. The input variables are: wind direction at 500 hPa in the model grid point closest to the examined region; vertical temperature gradient ΔT_1 in the same grid point; temperature differences ΔT_2 and ΔT_3 at 850 hPa in northeast-southwest and northwest-southeast direction, respectively.

(b) MLP (6, 8)

The second MLP consists of 6 inputs and 8 hidden units. Here, input variables are: latitude and longitude of the centers of the closest cyclone to Bulgaria at 850 hPa; wind speed at 500 hPa in the model grid point closest to the examined region; vertical temperature gradient ΔT_1 in the same grid point; temperature differences ΔT_2 and ΔT_3 at 850 hPa in northeast-southwest and northwest-southeast direction, respectively.

(c) MLP (5, 7)

The third MLP has 5 inputs and 7 hidden units. Variables here are: latitude and longitude of the centers of the closest cyclone to Bulgaria at 500 hPa; wind speed and wind direction at 500 hPa in the model grid point closest to the examined region; vertical temperature gradient ΔT_1 in the same grid point.

(d) MLP (27, 14)

MLP with all 27 variables and 14 hidden units was trained as well.

The performance of the neural networks for the cool season (*Table 1*) is higher than that of the warm season (*Table 2*), varying from 60 to 70%, with a few exceptions below and above but not far from this range. The mean for all regions is 64%. The lower performance during the warm season is consistent

with previous neural network studies of precipitation (e.g., *Hall et al.*, 1999) and other forecast systems (e.g., *Fritsch* and *Carbone*, 2004).

Table 1. Performance (%) of the MLPs for all regions for the cool season of year 2005 (from January to March and from October to December)

Regions	Performance (%)			
	MLP (7, 8)	MLP (8, 11)	MLP (5, 16)	MLP (27, 14)
1	75	69	75	74
2	76	63	78	72
3	68	60	64	69
4	74	69	76	80
5	75	69	74	73
6	66	54	65	64

Table 2. Performance (%) of the MLPs for all regions for the warm season of year 2005 (from April to September)

Regions	Performance (%)			
	MLP (4, 14)	MLP (6, 8)	MLP (5, 7)	MLP (27, 14)
1	69	62	69	62
2	63	58	63	63
3	62	58	55	55
4	70	67	77	65
5	70	68	64	58
6	65	60	68	59

3.3. Sensitivity analysis and skill measures

An interesting problem is to find the input variables, which are considered the most important by a particular neural network. The STATISTICA Neural Networks software provides an opportunity for us to address this problem by conducting sensitivity analysis. Sensitivity analysis can give important insights into the importance of individual variables, although it must be employed with some care, because the sensitivity analysis does not rate the usefulness of variables in an absolute sense. Consider, for example, the case where two input variables are not independent. Then, if either is eliminated the model may compensate, because the other still provides the key information. In this case, the sensitivity analysis may rate these variables as of low sensitivity, even

though they might encode key information. Similarly, a variable that encodes relatively unimportant information may have higher sensitivity than any other variables that encode more important information. If variable always has high sensitivity in various models, we can try to find some physical reason why this variable is so important for the model and what the nature of the dependence is between the input and output variables. Because of the complex relationships between the large-scale variables from NWP models and small-scale precipitation amounts, caution must be employed with sensitivity analysis.

Using sensitivity analysis, we selected a number of input variables for the different MLPs. For the cool season, 500 hPa wind speed and direction are presented in all MLPs. For the warm season, variables that are selected in all MLPs are the temperature difference between 850 and 500 hPa (ΔT_1) and the wind direction at 500 hPa. The vertical temperature difference (ΔT_1) is a measure of the static stability and the ingredients of the heavy precipitation (e.g., *Doswell et al.*, 1996).

Sensitivity analysis has been done on MLP (27, 14) as well, for the cool and warm seasons. The most important of all the 27 variables for classifying the precipitation cases obtained by averaging over all the regions are shown in *Table 3*. There is some difference for the cool and warm season, but temperature and wind variables seem to be the most important for the classification.

Table 3. Most important variables for the cool season and warm season

Cool season
Temperature difference at 850 hPa over Bulgaria in northwest-southeast direction
Temperature at 500 hPa in the model grid point closest to the geographic region
Wind direction at 850 hPa in the model grid point closest to the geographic region
Temperature at 850 hPa in the model grid point closest to the geographic region
Wind direction at 500 hPa in the model grid point closest to the geographic region
Longitude of the anticyclone closest to Bulgaria at 500 hPa
Wind speed at 850 hPa in the model grid point closest to the geographic region
Temperature difference at 850 hPa over Bulgaria in northeast-southwest direction
Temperature difference between 850 and 500 hPa in the model grid point closest to the geographic region
Latitude of the anticyclone closest to Bulgaria at sea level
Warm season
Wind direction at 500 hPa in the model grid point closest to the geographic region
Temperature difference at 850 hPa over Bulgaria in northwest-southeast direction
Temperature difference at 850 hPa over Bulgaria in northeast-southwest direction
Latitude of the closest to Bulgaria cyclone at 500 hPa
Mean sea level pressure at the center of the anticyclone closest to Bulgaria
Longitude of the cyclone closest to Bulgaria at 500 hPa
Longitude of the anticyclone closest to Bulgaria at sea level
Latitude of the anticyclone closest to Bulgaria at 500 hPa
Longitude of the anticyclone closest to Bulgaria at 500 hPa
Longitude of the anticyclone closest to Bulgaria at sea level

Hall et al. (1999) found, that the most significant variables in their neural network for precipitation forecasting for Dallas-Fort Worth, Texas, were the precipitable water and a number of variables closely related to the temperature and wind fields. Thus, our results are similar to that obtained in that study, taking into account the absence of the humidity as an input in our neural networks.

A receiver operating characteristic (ROC) curve (e.g., *Zweig* and Campbell, 1993; *Masters*, 1993) measures the performance of a two-class classifier. A ROC curve plots the hit rate versus the false alarm ratio. A random classifier, with no ability to discriminate between two classes, has a diagonal line ROC curve from (0,0) to (1,1). The classifiers with curves above the diagonal are skilled. The area under the curve is a scalar measure of the classifier's performance. The random classifier has an area of 0.5 under the ROC curve, whereas ideal classifiers have an area of 1 under the ROC curve.

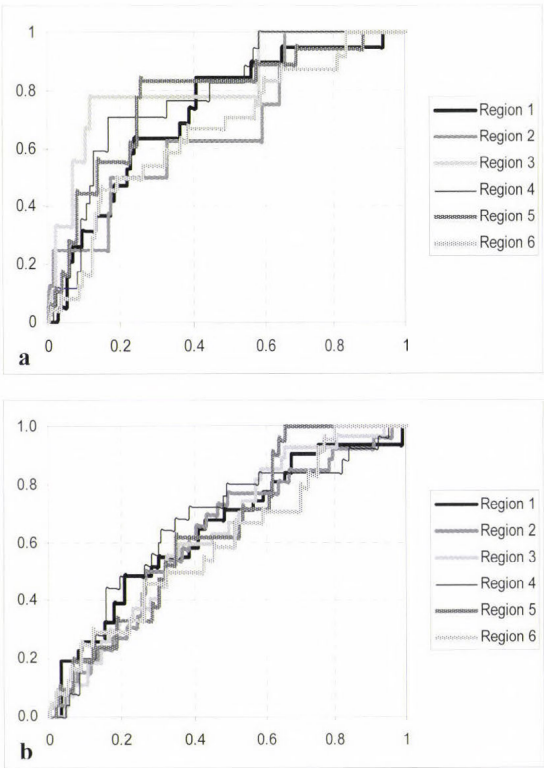

Fig. 2. ROC curves of the MLP (27, 14) for the cool (a) and warm (b) season of 2005.

ROC curves of the MLP (27, 14) for all regions in the cool and warm seasons (*Fig. 2*) show that the performance of the network in the cool season is much better than in the warm. For the cool season, ROC curves are closer to the

perfect classifier and the areas under the curves are larger than in the warm season. The performance of MLP (27, 14) is not the same for all regions. Areas under the ROC curves vary from region to region and from season to season (*Table 4*). The area averaged over all the regions for the cool season is 0.74 and for the warm season it is 0.64.

Table 4. Areas under the ROC curves of MLP (27, 14) for the cool and warm seasons of 2005

Region	Cool season	Warm season
1	0.72	0.65
2	0.68	0.63
3	0.80	0.63
4	0.78	0.66
5	0.78	0.65
6	0.67	0.61
Average	**0.74**	**0.64**

We defined an ensemble of the four MLPs for each season in the following way: when three of the four MLPs predict the precipitation amount to exceed the seasonal dependent threshold, then the ensemble issues the warning, otherwise there is no warning.

4. ALADIN NWP model and a combined system (ALADIN+ANN ensemble)

The total amount of precipitation in 2005 at the 40 Bulgarian stations was 130–170% of the annual average measured in the years 1961–1990 (*Fig. 3*).

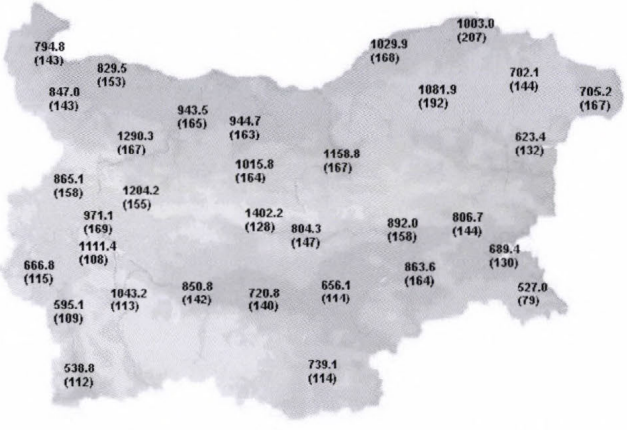

Fig. 3. Annual amount of precipitation (mm) for 2005 over Bulgaria and the percentage (in brackets) of the annual average for the period 1961–1990.

Heavy precipitation produced many flash floods, affecting most of the country, especially during the summer. Damage was extensive, and there were even casualties (*Gospodinov et al.*, 2006; *Stoicheva* and *Latinov*, 2006; *Hristov* and *Latinov*, 2006; *Georgiev* and *Santurette*, 2006). June and August were extremely wet months with monthly precipitation amounts exceeding 2–3 times the average values. The second wettest May–August period in Bulgaria since 1961 was 2005 (*Simeonov et al.*, 2006). Some verification results of precipitation event forecasting are presented here for ALADIN NWP model and for a combined system using ANN technique for the year 2005.

The ALADIN limited area NWP model has been built by the international collaboration between Météo-France and National Meteorological Services of Central and Eastern European countries and has been in operation in Bulgaria since 1999. Verification results for the year 2005 of ALADIN NWP model for precipitation predictions are presented in *Table 5*. Four skill scores are presented here. The first index presented here is the bias score (*BIAS*) defined as

$$BIAS = \frac{H + FA}{H + M}, \quad 0 \leq BIAS \leq \infty, \tag{1}$$

where H is the number of hits (the forecast system predicted the heavy precipitation event and it occurred), FA is the false alarms (the forecast system predicted the heavy precipitation event but it did not occurred), and M is the misses of the contingency table. This score measures the ratio of the frequency of forecasted events to the frequency of observed events.

Table 5. Bias score (*BIAS*, the perfect score is 1), Equitable threat score (*ETS*, the perfect score is 1), Hanssen and Kuipers discriminant (*HK*, the perfect score is 1), and odds ratio (*OR*, the perfect score is infinity) of the ALADIN NWP model (ALAD) and the combined system (ALAD + ANN) for the six regions in 2005

Region	BIAS		ETS		HK		OR	
	ALAD	ALAD+ANN	ALAD	ALAD+ANN	ALAD	ALAD+ANN	ALAD	ALAD+ANN
1	0.58	0.79	0.11	0.59	0.16	0.69	3.5	108.1
2	0.82	0.82	0.12	0.69	0.20	0.75	4.2	318.5
3	0.74	1.05	0.21	0.57	0.30	0.74	8.6	78.8
4	0.88	1.00	0.21	0.57	0.33	0.72	8.0	77.2
5	0.83	1.00	0.24	0.57	0.36	0.73	8.3	66.5
6	0.66	0.83	0.27	0.52	0.38	0.64	10.6	44.4
Avg.	**0.75**	**0.92**	**0.19**	**0.59**	**0.29**	**0.71**	**7.2**	**115.6**

The equitable threat score (Gilbert threat score) (*ETS*; *Gandin* and *Murphy*, 1992) is often used for verification of precipitation:

$$ETS = \frac{H - H'}{H + FA + M - H'}, \quad -1/3 \leq ETS \leq 1, \tag{2}$$

and it measures the fraction of observed and/or forecast events that were correctly predicted, adjusted for hits associated with random chance H'. H' is given as

$$H' = \frac{(H + FA)(H + M)}{N}, \tag{3}$$

where N is the total number of cases. The perfect score is $ETS=1$, while $ETS=0$ indicates no skill.

The Hanssen and Kuipers discriminant (*HK*; *Hanssen* and *Kuipers*, 1965) is defined as

$$HK = \frac{H}{H + M} - \frac{FA}{FA + CN}, \quad -1 \leq HK \leq 1, \tag{4}$$

where *CN* is the number of correct negatives (the forecast system predicted that the precipitation would be below the threshold and it occurred) of the contingency table. This score can be interpreted as a_1+a_2-1, where a is the accuracy for heavy precipitation events and a_2 is the accuracy for non-heavy precipitation events, and it shows how well a given forecast system separates the events of the two classes. The perfect score is $HK=1$, while $HK=0$ indicates no skill.

The last skill score presented here is the odds ratio (*OR*; *Stephenson*, 2000) defined as

$$OR = \frac{H \cdot CN}{M \cdot FA}, \quad -\infty \leq OR \leq +\infty, \tag{5}$$

measuring the odds of making a hit to the odds of making a false alarm.

To obtain better skill in forecasting heavy precipitation events we defined an ANN ensemble of the MLPs in the following way: when three of the four MLPs predict the precipitation amount to exceed the seasonal dependent threshold, then the ensemble issues the warning, otherwise there is no warning.

The second step is to create a combined system consisting of the ALADIN and ANN ensemble. This system works in the following way. First, the ALADIN model determines the precipitation events as those, when the model predicts precipitation amounts greater than a given threshold, here greater than 3 mm/12 hours. Since ALADIN overestimates precipitation events, the threshold is defined to minimize false alarms, and mountains are excluded from consideration as well. Second, as the precipitation event is predicted, the prediction of ANN ensemble is taking into account.

The combined system gives considerably better results than the ALADIN model alone in forecasting heavy precipitation events. The ALADIN NWP model underestimates heavy precipitation events. Although the combined system also shows tendency to underforecast heavy precipitation on average, the *BIAS* is much closer to 1. *ETS* gives clear indications that the combined system predicts more accurately heavy precipitation events than the ALADIN. *HK* shows that the combined system exceeds considerably the results of the ALADIN model in separating the two classes: heavy and non-heavy precipitation. Results for the *OR* indicate that the odds of correct heavy precipitation forecast for the combined system is several times greater than the odds calculated for the ALADIN model alone.

5. Conclusions

Successful application of the neural network technique for precipitation class distinction was presented. Two four-member sets of MLPs for cool and warm seasons were designed. The ROC curves showed good skill of the trained MLPs, although better in the cool season than in the warm season, consistently with previous results. Two reasons are possible for this performance. First of all, the dominant precipitation mechanisms during these two periods of the year are different. In summer, convective precipitation is dominant, in contrast to winter, when the precipitation is mainly stratiform. Second, convective precipitation might be local, but torrential. If the observing network is sparse, then such local precipitation might not be measured.

We found close relationship between certain input variables and the precipitation class through sensitivity analysis. The most important variables for cool and warm seasons are different, but temperature and wind variables are dominant.

We have showed that the combination of the ALADIN NWP model and the ANN ensemble gives better results than the NWP model alone. In this context, we succeeded in our objective to improve the forecasting of heavy precipitation combining NWP predictions with the classical synoptic approach.

Our technique could be improved in the following ways. First, the combinations of the input variables might not be unique. Perhaps, other combinations are possible. Other variables probably exist, which are not among these 27 inputs, but which may be very important for the precipitation process.

This paper is the first attempt to use neural networks for weather forecasting in Bulgaria, and the MLPs described in this paper could be applied to operational forecasting. This method should be used together with other forecasting data, such as the input from limited area NWP models, for achieving better results. Including the neural network technique in the forecasting process will help forecasters be more confident of issuing weather warnings. However,

because the neural network approach is not perfect, there is still a role for humans in the forecast process.

Acknowledgments—Thanks to *David Schultz* for providing very helpful comments to improve this manuscript. Thanks to *Pravda Dimitrova* for her courtesy in providing information about the annual precipitation amounts for 2005. We are grateful to *Plamen Neitchev* and *Anna Ghelli* who helped us improve this manuscript.

References

Banket, R., 1994: Cloud classification of AVHRR imagery in maritime regions using a probabilistic neural network. *J Appl Meteorol 33,* 909–917.

Bishop, C., 1995: *Neural Networks for Pattern Recognition.* Oxford University Press, 504 pp.

Chevallier, F., Morcrette, J.-J., Chéruy, F. and *Scott, N.A.*, 2000: Use of a neural-network-based long-wave radiative-transfer scheme in the ECMWF atmospheric model. *Q J Roy Meteorol Soc 126,* 761-776.

Doswell, C.A. III, Brooks, H.E. and *Maddox, R.A.*, 1996: Flash flood forecasting: An ingredients-based methodology. *Weather Forecast 11,* 560-581.

Fritsch, J.M. and *Carbone, R.E.*, 2004: Improving quantitative precipitation forecasts in the warm season: A USWRP research and development strategy. *B Am Meteorol Soc 85,* 955-965.

Georgiev, C. and *Santurette, P.*, 2006: MSG WV-channels. Exercises. Diagnosis of mid- to upper-level convection environment by using 6.2 μm and 7.3 μm images. *NIMH–EUMETSAT Workshop on MSG Applications in Nowcasting*, Sofia, Bulgaria, EUMETSAT, CD-ROM. [Available from C. Georgiev, Forecasting Department, National Institute of Meteorology and Hydrology, 66 Tsarigradsko Chaussee, Sofia 1784, Bulgaria.]

Ghelli, A., cited 2006: Verification of weather parameters. Available online at http://www.ecmwf.int/newsevents/meetings/forecast_products_user/Presentations2006/Ghelli.pdf.

Glahn, H.R. and *Lowry, D.A.*, 1972: The use of Model Output Statistics (MOS) in objective weather forecasting. *J Appl Meteorol 11*, 1203-1211.

Gandin, L.S. and *Murphy, A.H.*, 1992: Equitable skill scores for categorical forecasts. *Mon Weather Rev 120*, 361-370.

Gospodinov, I., Stoyanova, S. and *Dimitrova, P.*, 2006: Flood event in Bulgaria in August 2005 (the Ichtiman Cyclone). *Conf. on Water Obs. and Information Sys. for Decision Support.* Ohrid, Macedonia, BALWOIS, CD-ROM, A-204.

Hall, T., H. E. Brooks Doswell III, C.A.. 1999: Precipitation forecasting using a neural network. *Weather Forecast 3,* 338-345.

Hanssen, A.W. and *Kuipers, W.J.A.*, 1965: On the relationship between the frequency of rain and various meteorological parameters. *Meded. Verhand. K. Nederlands Meteor. Inst. 81,* 2-15.

Hristov, H. and *Latinov, L.*, 2006: Three situations in summer 2005 led to floods in Bulgaria (in Bulgarian). *Proc. First National Research Conf. on Emergency Management and Protection of the Population.* Sofia, Bulgaria, Bulgarian Academy of Sciences, 134-141

Lalaurette, F. and *van der Grijn, G.*, 2006: Ensemble forecasts: Can they provide useful early warnings? In *Predictability of Weather and Climate* (eds.: *T. Palmer* and *R. Hagedorn*). Cambridge University Press, 614-627.

Levenberg, K., 1944: A method for the solution of certain non-linear problems in least squares. *Q J Appl Math 2,* 164-168.

Marquardt, D.W., 1963: An algorithm for least-squares estimation of non-linear parameters. *J Soc Indust Appl Math 11,* 431-441.

Marzban, C., 2000: A neural network for tornado diagnosis. *Neural Comput Appl 9,* 133-141.

Masters, T., 1993: *Practical Neural Network Recipes in C++*. Academic Press, San Diego, 493 pp.

Parker, D.B., 1985: Learning logic. *Tech. Rep. TR-47,* Center for Comp. Research in Economics and Management Science, Massachussetts Institute of Technology, Cambridge, Massachussetts.

Rodwell, M.J., 2006: Comparing and combining deterministic and ensemble forecasts: How to predict rainfall occurrence better. *ECMWF Newsletter 106*, 17-23.

Roebber, P.J., Bruening, S.L., Schultz, D.M. and *Cortinas, J.V. Jr.*, 2003: Improving snowfall forecasting by diagnosing snow density. *Weather Forecast 18,* 264-287.

Rumelhart, D.E., Hinton, G.E. and *Williams, R.J.*, 1986: Learning internal representations by error propagation. In *Parallel Distributed Processing, Vol. 1* (eds.: *D.E. Rumelhart* and *J.L. McClelland*). MIT Press, 318-362.

Shepherd, A.J., 1997: *Second-Order Methods for Neural Networks: Fast and Reliable Training Methods for Multi-Layer Perceptrons*. Springer-Verlag, 145 pp.

Simeonov, P., Bocheva, L. and *Marinova, T.*, 2006: Assessment of the risk of hazardous convective weather during the warm half of the year (in Bulgarian). *Proc. First National Research Conf. on Emergency Management and Protection of the Population*. Sofia, Bulgaria, Bulgarian Academy of Sciences, 88-96.

Simmons, A.J. and *Hollingsworth, A.*, 2002: Some aspects of the improvement in skill of numerical weather prediction. *Q J Roy Meteor Soc. 128,* 647-677.

Stephenson, D.B., 2000: Use of the "odds ratio" for diagnosing forecast skill. *Weather Forecast 15*, 221-232.

Stoicheva, A., and *Latinov, L.*, 2006: Synoptical conditions in winter 2005 led to floods and snowstorms in particular regions of Bulgaria (in Bulgarian). *Proc. First National Research Conf. on Emergency Management and Protection of the Population*. Sofia, Bulgaria, Bulgarian Academy of Sciences, 211-219.

Werbos, P.J., 1974: Beyond regression: New tools for prediction and analysis in the behavioural sciences. *Ph.D. thesis*, Harvard University.

Wilby, R.L. and *Wigley, T.M.L.*, 1997: Downscaling general circulation model output: a review of methods and limitations. *Prog Phys Geog 21*, 530-548.

Xiao, R. and *Chandrasekar, V.*, 1997: Development of a neural network based algorithm for rainfall estimation from radar observations. *IEEE T Geosci Remote 35,* 160-171.

Zhanqing, L., Khananian, A., Fraser, R.H. and *Cihlar, J.*, 2001: Automatic detection of fire smoke using artificial neural networks and threshold approaches applied to AVHRR imagery. *IEEE T Geosci Remote 39,*1859-1870.

Zweig, M.H. and *Campbell, G.*, 1993: Receiver-Operating Characteristic (ROC) plots: A fundamental evaluation tool in clinical medicine. *Clin Chem 39,* 561-577.

IDŐJÁRÁS

Quarterly Journal of the Hungarian Meteorological Service
Vol. 114, No. 3, July–September 2010, pp. 169–185

Satellite-derived normalised difference vegetation index for monitoring climate impacts on European agriculture

Leonidas Toulios[1], **Gheorghe Stancalie**[2], **Elena Savin**[2], **F. Mark Danson**[3], **Piotr Struzik**[4], **Zoltán Dunkel**[5], and **János Mika**[6,7]

[1]*National Agricultural Research Foundation, 413 35 Larissa, Greece; E-mail: ltoulios@nagref.gr*
[2]*National Meteorological Administration*
013686, Bucharest, Romania; E-mail: gheorghe.stancalie@meteoromania.ro
[3]*Centre for Environmental Systems Research, University of Salford*
Manchester M5 4WT, UK; E-mail: f.m.danson@salford.ac.uk
[4]*Institute of Meteorology and Water Management*
P. Borowego Str. 14, 30-215 Krakow, Poland; E-mail: piotr.struzik@imgw.pl
[5]*Hungarian Meteorological Service*
P.O. Box 39, H-1675 Budapest, Hungary; E-mail: dunkel.z@met.hu
[6]*Hungarian Meteorological Service*
P.O. Box 38, H-1525 Budapest, Hungary; E-mail: mika.j@met.hu
[7]*Eszterházy Károly College, Department of Geography, Leányka u. 6, H-3300 Eger, Hungary*

(Manuscript received in final form September 21, 2009)

Abstract—Some of the climate and biophysical variables essential for understanding and monitoring the climate system and the impact of climate change on agriculture can be efficiently observed from orbital platforms, providing global data sets continuously and consistently. In order to describe the status of satellite–derived data useful for monitoring climate impacts on European agriculture, an initiative was started within the EU COST Action 734, for the registration and analysis of the relevant satellite data records, based on a specific questionnaire. It was noted that among European countries there are great differences concerning the climate and biophysical data derived from satellite measurements in terms of type, collecting period, spatial and spectral characteristics. However, in many countries satellite data have been collected systematically for several years, and these data records have proved to be useful for climate change impact studies in agriculture. The main variables that are collected in an operational or experimental way are land surface temperature and normalized difference vegetation index (NDVI). This paper presents case studies in three European countries, representing the current application stages in the field of the use of NDVI data in impact studies of climatic change on agriculture. Future research will assess the availability and quality of time series of spectral and biophysical data available from current satellite sensors. The main goal of this paper is to demonstrate the common research activity focused on NDVI and carried out in the frame of EU COST Action 734.

Key-words: NDVI, NOAA/AVHRR, SPOT/VEGETATION, vegetation state monitoring, drought monitoring, regionalization, European survey, COST/CLIVAGRI

1. Introduction

The main objective of EU COST Action 734 "Impacts of Climate Change and Variability on European Agriculture – CLIVAGRI" is the evaluation of possible impacts from climate change and variability on agriculture, and the assessment of critical thresholds for various European areas. This goal will be achieved through the accomplishment of intermediate aims, in order to assess the current and future levels of critical thresholds and hazards for agricultural activity and environmental resources. The activities of four working groups have been structured as a matrix, with the rows representing the methods of analysis and the columns the phenomena and hazards. Each intersection point describes the evaluation of past, present, and future trends of climate and so the impacts on agriculture. Based on these results, possible actions (specific recommendations, suggestions, warning systems) will be defined and proposed to the end users, depending on their needs. More details are available at: http://www.cost734.eu.

An important objective of Action 734 is to study the benefits of satellite remote sensing to assess climate change and variability impacts on agriculture. The research effort is directed towards the analysis of the role of satellite data in models and indices for assessing the impacts of climate change and variability on European agriculture. The type and distribution of vegetation in a given geographical region is diagnostic of the area's climate. This is because vegetation integrates the effects of precipitation and temperature over all time frames longer than a few days. In addition, the vegetation feeds back into climate through its effect on the surface energy budget and moisture balance and its impact on surface roughness and albedo. Vegetation index values, specifically the NDVI, calculated from reflectance recorded in red and NIR wavebands are often referred to as greenness values, because they are strong indicators of vegetation condition and quantity. For these reasons, NDVI time series allow monitoring of vegetation changes over seasonal to inter-annual time frames and over long periods, to monitor climate impacts on agriculture. The objectives of this study are to provide an overview of the underpinning principles behind the application of vegetation indices to assess climate change impacts, and to assess the current operational application of such methods at a European scale.

2. COST 734 pan-European survey

In order to describe the status of satellite climatic and biophysical data that are used for warning purposes for agriculture in Europe, an inventory (http://www.cost734.eu/working-group-2) was created through a questionnaire disseminated to the national delegates of COST 734 member countries (*Toulios et al.*, 2008). The analysis, based on the questionnaires returned by the COST 734 national delegates (15 European countries), shows a general interest in using

satellite climate and biophysical data and products to understand better how climate affects crop growth and yield, and for warning purposes in agriculture. Among European countries there is a great heterogeneity concerning the climatic and biophysical data received from satellite sensors or collected as satellite-derived ready products. Some countries have been collecting satellite data systematically for many years, and these data records could be useful for modeling in climate change impacts studies. Based on the distributed questionnaire, the 12 countries that use the variable NDVI are Austria, Bulgaria, France, Germany, Greece, Hungary, Italy, Poland, Romania, Slovenia, Spain, and Switzerland. The type of satellites and associated instruments are MODIS/TERRA-AQUA, AVHRR/NOAA, VEGETATION/SPOT, TM/LANDSAT, and SEVIRI/-METEOSAT.

Climate and biophysical variables are very relevant for monitoring vegetation status and predicting the possible impacts on crops. Some efforts are currently made by the remote sensing community to provide such products from medium spatial resolution satellite observations operationally available, including VEGETATION, MODIS, and AVHRR. However, the products are currently poorly validated because of the lack of ground measurements. In addition, most of the validation activities correspond to 'one shot' ground measurements, precluding access to the seasonality and associated phenology of the crops, even though most of the information on vegetation functioning lies in its dynamics.

Since the COST 734 survey revealed NDVI as one of the most widely used satellite-based variable in many European countries, this paper focuses on the use of NDVI time series imagery for monitoring climate impacts on agriculture. In this respect case studies in three European countries are presented.

3. Current status of satellite-derived NDVI in impact studies of climatic change on agriculture

Observations of spectral reflectance from remotely sensed data allow the quantitative characterization of terrestrial vegetation canopies. Efforts have been made to develop algorithms deriving surface properties from remotely sensed spectral reflectance or their end products. These include both empirical schemes, such as the spectral vegetation index (*Sellers et al.*, 1994; *Hall et al.*, 1995) and model inversion methods (*Pinty et al.*, 1990; *Privette et al.*, 1995; *Gao* and *Lesht*, 1997; *Danson et al.*, 2003).

The most relevant variables measured over land are solar radiation, daily global albedo, leaf area index (LAI), land surface temperature (LST), rainfall, evapotranspiration, cloud cover, fires and burned areas, snow cover, digital elevation maps of ice sheet surfaces, glacier evolution, and land cover. Some of these variables are required as inputs to give an immediate view of climate

change impacts, for example (*Struzik et al.*, 2008). They are also widely used as inputs to agrometeorological models (*Struzik*, 2005; *Stancalie et al.*, 2006). The most important parameters derived from vegetation indices are the maximum greenness during the growing season, total greenness during the growing season, fraction of photosynthetically active radiation (FPAR), absorbed photosynthetically active radiation (APAR), and leaf area index (LAI).

Various remote-sensing-based studies have revealed persistent spectral relationships between the red and near-infrared (NIR) reflectance and the amount of green vegetation. Due to vegetation pigment absorption (chlorophyll, proto-chlorophyll), the reflected red energy decreases, while the reflected NIR energy increases as a result of the strong scattering processes of healthy leaves within the canopy. Directly using the amount of reflected red and/or NIR radiation to study the biophysical characteristics of vegetation is normally inadequate, for reasons rooted in the intricate radiative energy interactions between the canopy, soil background, atmosphere, and the non-uniqueness of the signatures. When, however, two or more bands are combined into a vegetation index (VI), the vegetation related component of the signal is boosted and the information becomes more useful. VIs can therefore be used as an indirect measure of vegetation activity.

Many VIs have been reported in the literature and some have proved to be well correlated with vegetation biophysical parameters. Tremendous efforts have been devoted to improve VI and render them insensitive to variations in illumination conditions, observing geometry, and soil properties. Even though the external perturbing factors related to changes in soil brightness and atmospheric conditions may be taken into account, VI still have definite intrinsic limitations; they are not a single measure of a specific variable of interest such as pigment content, plant geometry, or canopy architecture. So far, it has not been possible to design an index which is sensitive only to the desired variable and totally insensitive to all other vegetation parameters.

Therefore, different indices have been defined for different purposes, and optimized to assess a process of interest. For instance, some spectral indices have been proposed to capture the photochemical processes associated with photosynthetic activity such as light use efficiency or to estimate leaf pigment content (*Kim et al.*, 1994; *Broge* and *Leblanc*, 2000; *Daughtry et al.*, 2000; *Haboudane et al.*, 2002). A major problem in the use of these indices arises from the fact that canopy reflectance, in the visible and NIR, is strongly dependent on both structural (e.g., LAI) and biochemical properties (e.g., chlorophyll content) of the canopy (*Jacquemoud et al.*, 2000; *Zarco-Tejada et al.*, 2001).

LAI and chlorophyll content have similar effects on canopy reflectance, particularly in the spectral region from the green (550 nm) to the red edge (750 nm). To uncouple their combined effect, recent research studies (*Daughtry et al.*, 2000; *Haboudane et al.*, 2002) have demonstrated that leaf chlorophyll

content can be estimated with minimal confounding effects due to LAI through a combination of two kinds of spectral indices: indices sensitive to pigment concentration and indices resistant to soil optical properties influence.

Other studies have dealt with modifying VIs to improve their linearity with, and increase their sensitivity to, LAI (*Haboudane et al.*, 2004a). Consequently, some indices have been identified as 'best' estimators of vegetation biophysical parameters, because they are less sensitive to the variation in external parameters affecting the spectral reflectance of the canopy, namely soil optical properties and atmospheric conditions (*Broge* and *Leblanc*, 2000), as well as to changes in leaf intrinsic properties such as chlorophyll concentration (*Haboudane et al.*, 2004b).

The most widely used form of VI, the normalized difference vegetation index, was introduced by *Deering* (1978) and *Tucker* (1979) and is the ratio of the difference of the NIR and red reflectance divided by their sum. The NDVI mitigates a large part of the variations that result from the overall remote-sensing system (radiometric, spectral, calibration, noise, viewing geometry, and changing atmospheric conditions). NDVI is often used as a monitoring tool for vegetation health and dynamics, enabling easy temporal and spatial comparisons. In order to make effective use of NDVI data, issues related to the remote-sensing system need to be addressed. Most serious are clouds, which render any observation unusable by obstructing the target, and, to a lesser degree, the effects of the bidirectional reflectance distribution function (BRDF). To overcome these impediments, the maximum value compositing was developed as an operational approach to producing cloud free consistent NDVI images. Multiple daily images are processed to create a representative, cloud-free image with the least atmospheric attenuation and viewing geometry effects (*Holben*, 1986). The maximum value compositing (MVC) technique is the most widely used method based on maximizing the NDVI signal over a preset period of time (e.g., 16 days). Whilst the MVC helps screen for clouds, it has been found also to favor extreme viewing geometry (large solar zenith angles and large view angles in the forward scatter direction) and, to a lesser extent, cloud shadow. Several studies have attempted to address these issues (*Roujean et al.*, 1992; *Meyer et al.*, 1995; *Leeuwen et al.*, 2006).

Several factors can influence differences in NDVI computed from different satellite sensors. Impacts from BRDF are well documented (*Roujean et al.*, 1992; *Walter-Shea et al.*, 1997) and in addition, the spectral response functions for different sensors can lead to systematic differences in NDVI (*Trishchenko et al.*, 2002). Each sensor has its own instantaneous field of view, swath width, and orbiting geometry. Adjusting for these known differences is somewhat problematic and, in many cases, beyond the capability or resources available to many users (*Linthicum et al.*, 1999). *Table 1* presents the most widely used NDVI datasets, including information on sensor type, data source, spatial and temporal resolutions, equatorial crossing time, and field of view for each sensor.

Table 1. The most widely used NDVI datasets

Sensor	AVHRR	SPOT/ VEGETATION	MODIS	SeaWiFS	LANDSAT ETM+
Data source	GIMMS NDVIg operational dataset	FAS-GIMMS VITO	MODIS Land and Vermote/ Saleous	SeaWiFS/GS F/GIMMS	EOS web
Spatial resolution	800 m and 1 degree	1000 m and 1 degree	500 m 5000 m and 1 degree	4633 m 1 and 1 degree	30 m
Temporal resolution	15 days and monthly	10 days and monthly	16 days and monthly	monthly	16 days and monthly
Equatorial crossing	9 AM - 6 PM	10:30 AM	10:30 AM	12:05 PM	10 AM
Field of view	+/- 55.4°	+/- 101°	+/- 55°	+/- 58.3°	+/- 15.5°

An analysis made by *Brown et al.* (2007) revealed that, although relatively large differences existed between the mentioned NDVI datasets, the NDVI anomalies exhibited similar variances. Composite NDVI images are quite robust, which can be seen when comparing time series data with NDVI from LANDSAT ETM+ images that have been corrected for atmospheric effects.

Bai et al. (2004) generated an NDVI data set to provide a satellite record of monthly changes in terrestrial vegetation, using NOAA/AVHRR data. The NDVI trend in Europe was analyzed by taking representative pixels of each land use type. Generally, an increasing trend in NDVI in Europe is shown over the past 21 years (1982–2002). The increase of NDVI ranges from 0.03% to 0.2% per year (*Fig. 1*). The variations in NDVI of the different land use types over certain months in a year were observed. The variations were mainly due to the annual growth cycle of the vegetation. Characteristic features of specific land use types were visible in the variation of NDVI, like the harvesting of agricultural land, the loss of leaves in broad-leaved forests, and the persistent greenness of evergreen coniferous forests.

Satellites have different repeat cycles, which means that some satellites may provide only two images per month, whereas others can produce an image every day. This can have considerable impact on agricultural applications, since the repeat cycle characteristics of satellites are, for example, one of the determinants for forecasting yield using the NDVI. In addition, these high repeat cycle platforms usually have lower spatial resolution, influencing the appropriateness of its data to fine-scale applications. Another major cause of variation in the availability of optical data is cloud coverage. This could be problematic when the timing of image acquisition is critical as in crop identification. However, it may be avoided by using short-time compositing

synthesis that is available. In the case of NDVI, the highest value of the considered time period is chosen.

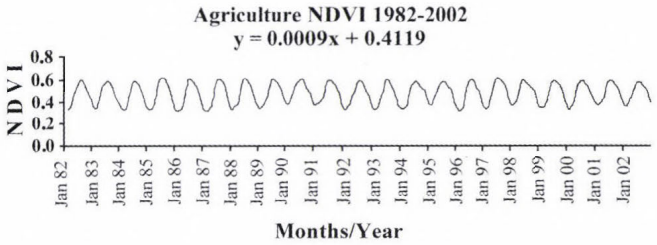

Fig. 1. Agriculture NDVI changes in Europe during 1982–2002 (*Bai et al.*, 2004).

3.1. Temporal resolution

It is important to get the right balance between the temporal resolution of data and the timescale of variation in the quantity measured. For example, maximum value composites of NDVI data are rarely less than decadal. Consequently, NDVI MVC should not be used to investigate short-term events. It is more appropriate to use NDVI data to monitor events of longer duration like the growth of vegetation through a season.

3.2. Atmospheric interference

Light scattering tends to increase the amount of red radiation received by the satellite as red is more readily scattered in the atmosphere than near infrared. This induces a reduction in the NDVI values. For short periods, this problem is minimized by taking the maximum value composite, because each pixel's maximum value is likely to have occurred when scattering was at a minimum.

3.3. Land cover type

With the exception of very large irrigation schemes and large area commercial agriculture, an NDVI pixel rarely covers a single, homogeneous cover type of agricultural land. Instead it may cover roads, buildings, bare soil, small water bodies, natural vegetation, and different agricultural crops, all within one pixel. In an NDVI image, one pixel is the weighted sum of the radiation reflected from all the land cover types within the area covered by the pixel. NDVI is an indicator of the condition of the overall vegetation in an area, including natural vegetation and crops. In rain-fed agriculture, natural vegetation may follow patterns similar to those of the crops. More often, however, agricultural crops are more susceptible to adverse conditions and follow different growth cycles.

3.4. Soil-type

Light reflected from the soil can have a significant effect on NDVI values (changing the values by up to 20%). Generally, the greater the reflectance of the soil is, the lower the NDVI values are. Soil-type is, therefore, an important factor. Given two soil types, the one with a greater reflectivity but with similar vegetative conditions, will on average produce lower NDVI values.

3.5. Off-nadir viewing effects

As the radiometer scans across the Earth, there is only one point, in the centre of the scan that is directly underneath the radiometer (called the sub-satellite point or nadir). The distance from the radiometer to the ground increases away from the sub-satellite point. This results in increased atmospheric interference as the light must pass through more atmosphere before reaching the radiometer, and, therefore, in reduced NDVI values. These effects are minimized by simply dropping the pixels at large off-nadir view angles.

4. Case studies

4.1. Time series of SPOT/VEGETATION NDVI for monitoring crop status in Romania

The agrometeorological activity of the Romanian National Meteorological Administration (RNMA) integrates complex topics concerning the current and future development of the phenological stages of the crops and soil moisture supply with respect to trends in meteorological parameters. This is a particularly important activity whose final objective is to provide information to the agro-meteorological bulletins and disseminate information to the level of the agricultural decision makers.

From 2005, the RNMA has benefitted from data provided by the SPOT/VEGETATION sensor (transmitted in quasi real time via FTP, as well as archived data) for better operational surveillance of agricultural areas. VGT-S10 products (ten-day synthesis) are compiled by merging segments acquired during a ten-day period. These products provide data from all spectral bands, the NDVI and auxiliary data on image acquisition parameters. An MVC synthesis can be also obtained at several different spatial resolution levels (1×1 km^2, 4×4 km^2, or 8×8 km^2).

The VGT-S10 products, namely decadal NDVI and color synthesis of composites, allow for crop state monitoring and analysis by using NDVI time series. Other more complex vegetation indices are derived, like the modified soil vegetation index (MSAVI) and vegetation condition index (VCI), by correlating

with various agrometeorological parameters provided by the national weather network.

- The key stages for crop state analysis, based on NDVI data series are: overlay of a mask in order to isolate agricultural land,
- overlay of reference points,
- selection of representative crop-cultivated areas with at least 4 km2 surfaces (equivalent of 4 pixels) using terrain information or high resolution satellite-derived land cover maps,
- accurate localization of the reference points using GPS,
- extraction of NDVI values.

The method developed for agricultural drought monitoring includes the following main steps:

- Deriving the NDVI values for each decade for each study area.
- Smoothing the data series using a moving temporal window and linear regression.
- Averaging the value of this linear function using various interpolation functions of a higher order.
- Comparing the yearly data series to observe a trends caused, for example, by the growth of the vegetation. Small differences caused by long-term fluctuations of climatic conditions in some regions can be highlighted as well.
- Using the multiyear NDVI minima and maxima, the values are forced into the same range and are made quantitatively comparable afterwards. This complex parameter is the vegetation condition index (VCI) given by

$$VCI=(NDVI-NDVI_{min})/(NDVI_{max}-NDVI_{min})\cdot 100. \quad (1)$$

The whole algorithm is applied for every pixel of the satellite image. In research by the Remote Sensing Team of the Romanian National Meteorological Administration (*Kianicka et al.*, 2007), this algorithm was applied using a time series of SPOT/ VEGETATION NDVI for a test area, situated in Arges County located in the southern part of Romania.

The latest generation of SPOT satellites is well known for their high-resolution imagery that is useful in agriculture, urban planning, forest management, monitoring and surveillance, etc. Considering the need for data with higher temporal resolution covering the whole globe, the new generation of satellites carries the VEGETATION instrument with a spatial resolution of 1 km and a

swath width of 2250 km which is able to image the whole of the Earth's surface on a daily basis. With its four channels, the sensor may be used to derive various secondary products. They are well suited to mapping vegetation over large areas and for global change studies.

In this application, the raw data are geometrically and atmospherically corrected and geo-referenced. The ten-day syntheses are also available. The original data are contaminated by clouds and weather fluctuations. In order to avoid this phenomenon as much as possible, short-time syntheses are generated. In the case of NDVI, the highest value of ten available images is chosen. Nevertheless, the cloudy parts are still presented, but are assigned specific values.

First, the data are smoothed, VCI indices are computed for each year, and the differences from the average value in this case are evaluated. These differences generate the first information about the behavior of drought in the study area. Applying a threshold, the potential map of drought stress can also be derived. *Fig. 2* presents the co-plot of VCI annual curves of the 1998–2005 decadal values, for a test area situated in Arges County. The computation of VCI has been restricted only to the crop growing season from April to the beginning of November.

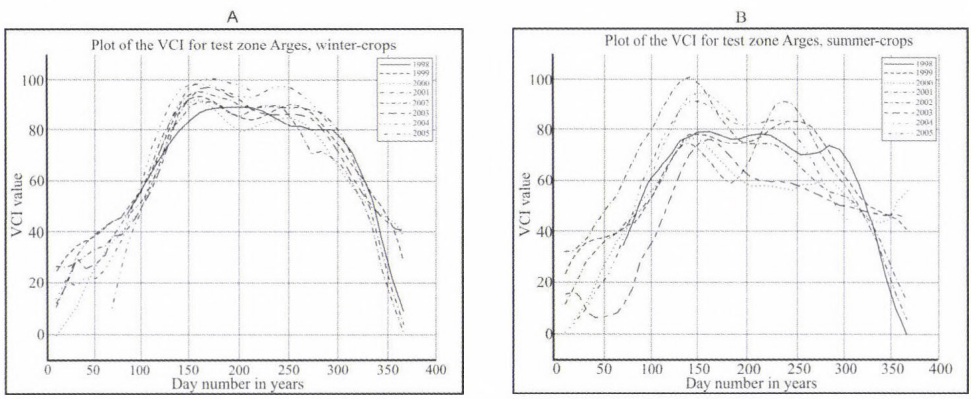

Fig. 2. Co-plot of annual VCI curves for winter (A) and summer crops (B).

The difference between winter and summer crops is clear; the summer crops have a more marked dispersion of values. In the drought years, 2000 and 2003, the cereal production of Romania was seriously reduced by drought, similarly to the reduced VCI values during summer. The co-plot of VCI curves and, consequently, the co-plot of differences regarding the linear-regression-in-time values (*Fig. 3*) confirm the results connected to monitoring of cereal output, temperature, and soil moisture.

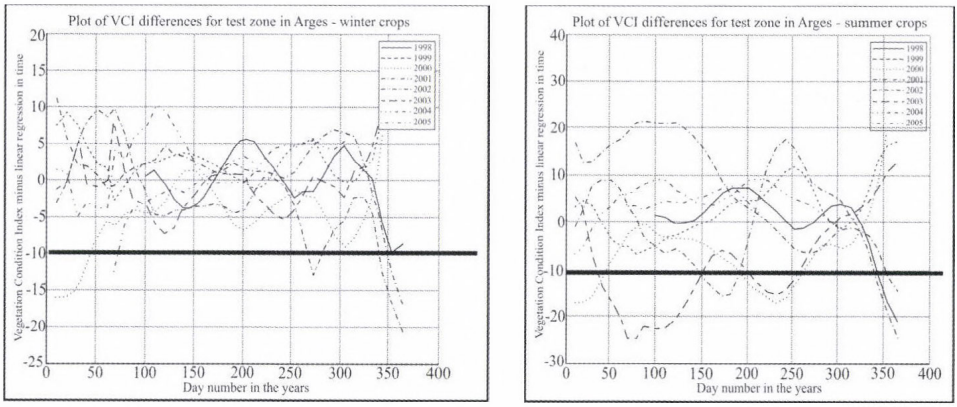

Fig. 3. Differences between original decadal value and linear-regression-in-time values for the winter and summer crops.

4.2. Vegetation indices for drought monitoring and crop damage assessment in Poland

Drought is the most important weather-related natural disaster. Droughts cannot be avoided, but although predictions will never be perfect, we can reduce their impacts. Large-scale intensive droughts have been observed on all continents, leading to massive economic losses, destruction of ecological resources, food shortages, and starvation of millions of people.

Reduction of drought consequences requires proper drought prediction, early warning and monitoring, to help with proper agricultural practices and decisions. Monitoring the impacts and extent of drought is also important for insurance companies. Lessons learned during an event may help in proper planning of irrigation systems. Thus, satellite information may have a substantial impact on improved drought management strategies (*Struzik*, 1991 and 1992). Its use in drought monitoring and early warning requires retrieval and monitoring of parameters such as:

- Rainfall, surface wetness, and temperature monitoring. Multi-channel and multi-sensor data sources from geostationary platforms (such as GOES, METEOSAT, GMS) and polar orbiting satellites (such as NOAA, DMSP SSMI, METOP, SMOS, GPM) have been used. Estimated indices describing actual atmosphere and surface conditions and also quantities useful for forecasting are precipitation intensity, amount, and coverage, surface soil wetness indices, atmospheric moisture content, wind speed and direction.

- Vegetation condition monitoring is currently possible, ranging from NOAA AVHRR data at 1.1 km resolution on a daily revisit from each satellite, to environmental satellites (LANDSAT etc.) on a 8–16 days revisit with a 10–30 m spatial resolution or even very high spatial resolution missions like IKONOS, QuickScat, etc. with resolutions of 0.6–4 m. The normalized difference vegetation index (NDVI), associated vegetation conditions index (VCI), and temperature condition index (TCI) derived from the satellite data are accepted worldwide for regional monitoring.
- Assessment of drought impact by high-resolution satellite sensors from LANDSAT, SPOT, and other high resolution satellites are being used for the assessment of impacts, but in most cases this is not a country-wide activity, mainly due to high costs of such information.

Examples of vegetation anomalies in Poland connected with severe drought conditions are presented in *Fig. 4*. NDVI indices were calculated from NOAA/AVHRR data, using the MVC for selected periods. Year 1992 was extremely dry in Poland, preceded by two dry years 1990 and 1991. Monthly precipitation amounts in Wielkopolska and South Pomeranian regions (dark on satellite NDVI image) were well below the long term monthly means. At some stations, precipitation in all months of the year was well below the long term mean (*Table 2*). June precipitation was less than 10% of the monthly mean followed by a very dry July, which resulted in severe drought lasting into late summer. The observed satellite-derived NDVI reached a minimum in August after four dry months.

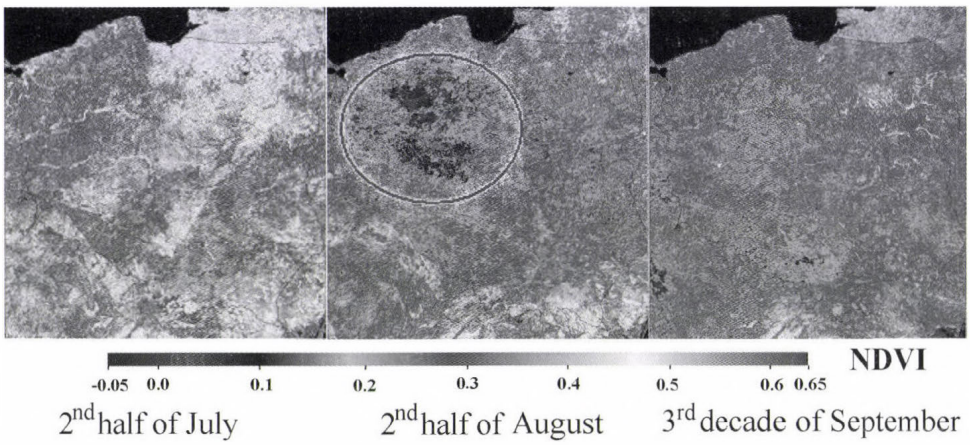

Fig. 4. Vegetation indices during the severe drought in Poland (1992).

Table 2. Monthly precipitation recorded at three selected synop stations during the drought in 1992, in comparison with climatological means for this region

Month	Monthly precipitation in 1992 for selected stations [mm]			Climatological mean for region [mm]
	Poznan	Chojnice	Pila	
April	18.3	31.7	16.4	31.3
May	27.6	31.0	25.7	47.1
June	3.4	36.8	7.9	61.9
July	24.7	36.7	23.1	76.0
August	45.6	43.2	39.6	55.4
September	15.4	32.4	26.4	43.6
Amount for season April–September	**135.0**	**211.8**	**139.1**	**315.3**

4.3. Using vegetation indices for objective regionalization in Hungary

The NDVI was derived from the NOAA/AVHRR sensor for a 14-year period, 1985–1998. The March–October vegetation growth period was further selected representing two-thirds of the year. Since yield data were available only on a county-wide basis, the NDVI series were also averaged over the 19 administrative counties, characterized by 50–90 km of linear size. The integration time step was one week, since under the climatic conditions of the country there is likely to be one cloud free day per week (*Mika et al.*, 2002).

Weekly NDVI data during the vegetation growth periods of 14 years from each of these 19 counties were subjected to a cluster analysis to characterize similarity or dissimilarity among the 19 administrative counties of Hungary. The aim was to find coherent groups of counties to unify them into larger, cumulative samples. More specifically, hierarchical joining based on Euclidean distance was used. The amalgamation was performed by the Ward's method (*Ward*, 1963), which used an analysis of variance approach to evaluate the distances between clusters. The result of the cluster analysis did not yield a strictly determined number of classes, but it is reasonable to rely on the stability of the classification which can be characterized by the average linkage distance between the classes. When a change in this linkage distance does not change the number of classes, the number of classes may be considered as stable. In this case, of the 19 counties, the most stable number of classes was 3 (*Fig. 5*). The remarkable feature of this objective classification is the west-east differentiation, with no clear north-south differences over counties in the NDVI values.

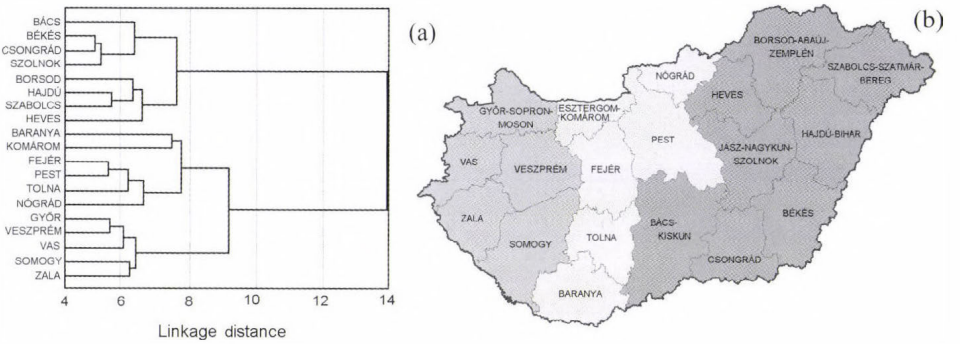

Fig. 5. Results of cluster analysis to determine objective vegetation regions in Hungary. The left axis of part (a) indicates the clustering process with the short names of the administrative counties in the order of their amalgamation. Part (b) indicates the three regions for which a stable linkage distance can be obtained.

5. Conclusions

For the past decade, newer and more sophisticated remote sensing systems have become operational providing biophysical measurements that are aimed at addressing monitoring climate impacts in European agriculture. Based on these advances, the use of multispectral satellite data allows improvement of the classical determination methods for agrometeorological parameters of interest. The most important advantages are related to the improvement in the spatial resolution in the range of meters to kilometers, as well as the frequency of updating with a temporal resolutions varying from hours to seasons.

A new generation of EUMETSAT space sensor systems presents a real opportunity to improve our knowledge of surface processes on a short-term basis. Instruments (like SEVIRI on the board of MSG, AVHRR-3 on the board of NOAA, and future EPS/METOP) will offer the opportunity to follow vegetation changes on a daily time scale, due to a high temporal resolution and more appropriate spectral bands to assess vegetation status. They will also provide data with multiple surface illumination angles that will bring new insights to our knowledge of the anisotropic surface reflectance properties. However, to achieve any meaningful monitoring of the land surface vegetation, stable, inter-calibrated long-term vegetation records (a decade or longer) are a key requirement. Progress can be made towards a unified NDVI dataset given that absolute variances across sensors are relatively similar, especially when seasonality is removed. Examples of the successful use of long time series of satellite data for monitoring climate impacts on agriculture in three European countries have been presented here together with an assessment of the limitations of the technology.

There is a need for additional research to improve the long-term data series record and addressing cross-sensor NDVI continuity. Good examples of the potential application could be the satellite image series of summer droughts of 2003, 2005, and 2006 in France. Among others, the NDVI deviations based on VEGETATION/SPOT 5 data could give very useful time series. Another good example would be the 2003 heatwave at the European scale (July 2003/July 2002). The initial results of the COST 734 inventory show an incomplete snapshot of the situation in the different countries across Europe. The gaps show the importance of pan-European collaboration on the collection, archiving and analysis of satellite derived data on variables related to climate change and agriculture.

References

Bai, Z., van Barneveld, B., Laita, E.L., Mengesha, T. and *Morelissen, B.*, 2004: Trends in NDVI changes in Europe using a 21 year satellite record. Poster submitted in partial fulfilment of the course Academic Master Cluster Environmental Sciences, part II. Wageningen UR, May 2004.

Broge, N.H. and *Leblanc, E.*, 2000: Comparing prediction power and stability of broadband and hyperspectral vegetation indices for estimation of green leaf area index and canopy chlorophyll density. *Remote Sens Environ 76*, 156-172.

Brown, M.E., Pinzón, J.E., Didan, H., Morisette, J.T. and *Tucker, C.J.*, 2007: Evaluation of the consistency of long-term NDVI time series derived from AVHRR, SPOT-vegetation, SeaWiFS, MODIS, and LandSAT ETM+ sensors. *IEEE T Geosci Remote 44*, 1787-1793.

Danson, F.M., Rowland, C.S. and *Baret, F.*, 2003: Training a neural network to estimate crop leaf area index. *Int J Remote Sens 24*, 4891-4905.

Daughtry, C.S.T., Walthall, C.L., Kim, M.S., Brown de Colstoun, E. and *McMurtrey III, J.E.*, 2000: Estimating corn leaf chlorophyll concentration from leaf and canopy reflectance. *Remote Sens Environ 74*, 229-239.

Deering, D.W., 1978: *Rangeland Reflectance Characteristics Measured by Aircraft and Spacecraft Sensors*. College Station, TX, Texas A&M University, p. 338.

Gao, W. and *Lesht, B.M.*, 1997: Model inversion of satellite-measured reflectances to obtain surface biophisical and bidirectional reflectance characteristics of grassland. *Remote Sens Environ 59*, 461-471.

Haboudane, D., Miller, J.R., Pattey, E., Strachan, I. and *Zarco-Tejada, P.J.*, 2002: Effects of chlorophyll concentrations on green LAI prediction in crop canopies: modelling, validation and heterogeneity assessment. *First International Symposium on the Recent Advances In Quantitative Remote Sensing*. Valencia, Spain, 16-20 September 2002.

Haboudane, D., Miller, J.R., Tremblay, N., Pattey, E. and *Vigneault, P.*, 2004a: Estimation of leaf area index using ground spectral measurements over agriculture crops: prediction capability assessment of optical indices. *Proc. of the ISPRS Symposium*, Istanbul, Turkey.

Haboudane, D., Miller, J.R., Pattey, E., Zarco-Tejada, P.J. and *Strachan, I.*, 2004b: Hyperspectral vegetation indices and novel algorithms for predicting green LAI of crop canopies: modeling and validation in the context of precision agriculture. *Remote Sens Environ 90*, 337-352.

Hall, F.G., Townshend, J.R. and *Engman, E.T.*, 1995: Status of Remote Sensing Algorithms for Estimation of Land Surface State Parameters. *Remote Sens Environ 51*, 138-156.

Holben, B., 1986: Characteristics of maximum-value composite images from temporal AVHRR data. *Int J Remote Sens 7*, 1417-1434.

Jacquemoud, S., Bacour, C., Poilve, H. and *Frangi, J.-P.*, 2000: Comparison of four radiative transfer models to simulate plant canopies reflectance: Direct and inverse mode. *Remote Sens Environ 74*, 417-481.

Kianicka, J., Savin, E., Flueraru, C. and *Craciunescu, V.*, 2007: Remote sensing data analyses for the study of drought. *Symposium GIS,* Ostrava, 28-31 Jan. 2007.

Kim, M.S., Daughtry, C.S.T., Chappelle, E.W., McMurtrey III, J.E. and *Walthall, C.L.*, 1994: The use of high spectral resolution bands for estimating absorbed photosynthetically active radiation (Apar). *Proc. of the 6th Symp. on Physical Measurements and Signatures in Remote Sensing.* Val D'Isere, France, Jan. 17-21, 1994, 299-306.

Leeuwen, W., Orr, B.J., Marsh, S.E. and *Herrmann, S.M.*, 2006: Multisensor NDVI data continuity: uncertainties and implications for vegetation monitoring applications. *Remote Sens Environ 100*, 67-81.

Linthicum, K.J., Anyamba, A., Tucker, C.J., Kelley, P.W., Myers, M.F. and *Peters, C.J.*, 1999: Climate and satellite indicators to forecast Rift Valley Fever epidemics in Kenya. *Science 285*, 397-400.

Meyer, B., Verstraete, M.M. and *Pinty, B.*, 1995: The effect of surface anisotropy and viewing geometry on the estimation of NDVI from AVHRR. *Remote Sens Rev 12*, 3-27.

Mika, J., Kerényi, J., Rimóczi-Paál, A., Merza, Á., Szinell, C. and *Csiszár, I.*, 2002: On correlation of maize and wheat yield with NDVI: example of Hungary (1985–1998). *Adv Space Res 30*, 2399-2404.

Pinty, B., Verstraete, M.M. and *Dickinson, R.E.*, 1990: A physical model of the bidirectional reflectance of vegetation. *J Geophys Res 95*, 11767-11775.

Privette, J.L., Myneni, R.B., Emery, W.J. and *Pinty, B.*, 1995: Inversion of a Soil Bidirectional Reflectance Model for use with vegetation reflectance models. *J Geophys Res 100*, 25497-25508.

Roujean, J.-L., Leroy, M., Podaire, A. and *Deschamps, P.Y.*, 1992: Evidence of surface reflectance bidirectional effects from a NOAA/AVHRR multitemporal data set. *Int J Remote Sens 13*, 685-698.

Sellers, P.J., Los, S.O., Tucker, C.J., Justice, C.O., Dazlich, D.A., Collatz, G.J. and *Randall, D.A.*, 1994: A global 1 by 1 degree NDVI data set for climate studies. Part 2: The generation of global fields of terrestrial biophysical parameters from the NDVI. *Int J Remote Sens 15*, 3519-3545.

Stancalie, G., Struzik, P. and *Toulios, L.*, 2006: Use of data from remote sensing as input for agrometeorology. In *COST Action 718, Metorological Applications for Ariculture*, COST Office, Brussels, 47-80.

Struzik, P., 1991: Seasonal changes of the NDVI over Poland. *Proc. of Fifth AVHRR Data Users Meeting*. Tromso 25-28, June 1991. EUMETSAT P 09, ISBN 92-9110-003-X, 77-82.

Struzik, P., 1992: Application of AVHRR/NOAA satellite information for monitoring of river basins surface parameters. *Proc. of Int. Conf. Operational Hydrology*. Wola Zręczycka, 21-22 Sept. 1992, 65-74.

Struzik, P., 2005: Possibilities for use of satellite information as an input for CROPWAT software - preliminary study. In *Use and Availability of Meteorological Information from Different Sources as Input in Agro-meteorological Models*. European Commission, DG XII, COST Action 718, 339-361.

Struzik, P., Toulios, L., Stancalie, G., Danson, M., Mika, J. and *Domenikiotis, C.*, 2008: Satellite remote sensing as a tool for monitoring climate and its impact on the environment - Possibilities and limitations. In *Survey of Agrometeorological Practices and Applications in Europe Regarding Climate Change Impacts*. COST, European Science Foundation, 205-236.

Toulios, L., Stancalie, G., Struzik, P., Danson, M., Mika, J., Dunkel, Z. and *Tsiros, E.*, 2008: Satellite spectral, climatic and biophysical data for warning purposes for european agriculture. In *Survey of Agrometeorological Practices and Applications in Europe Regarding Climate Change Impacts*. COST, European Science Foundation, 163-204.

Trishchenko, A.P., Cihlar, J. and *Li, Z.*, 2002: Effects of spectral response function on surface reflectance and NDVI measured with moderate resolution satellite sensors. *Remote Sens Environ 81*, 1-18.

Tucker, C.J., 1979: Red and photographic infrared linear combinations for monitoring vegetation. *Remote Sens Environ 8*, 127-150.

Zarco-Tejada, P.J., Miller, J.R., Noland, T.L., Mohammed, G.H. and *Sampson, P.H.*, 2001: Scaling-up and model inversion methods with narrow-band optical indices for chlorophyll content

estimation in closed forest canopies with hyperspectral data. *IEEE Trans Geosci Remote Sens 39*, 1491-1507.

Walter-Shea, E.A., Privette, J.L., Cornell, D., Mesarch, M.A. and *Hays, C.J.*, 1997: Relations between directional spectral vegetation indices and leaf area and absorbed radiation in alfalfa. *Remote Sens Environ 61*, 162-177.

Ward, J.H., 1963: Hierarchical grouping to optimize an objective function. *J American Stat Assoc 58*, 236-300.

Internet sources

http://www.cost734.eu and http://www.cost734.eu/working-group-2 (both available on 15 September, 2009)

IDŐJÁRÁS

Quarterly Journal of the Hungarian Meteorological Service
Vol. 114, No. 3, July–September 2010, pp. 187–201

Analysis of precipitation on Lake Balaton catchments from 1921 to 2007

Angéla Anda[*1] and **Balázs Varga**[2]

[1]*Department of Meteorology and Water, University of Pannonia Georgikon Faculty*
H-8360 Keszthely, Hungary; E-mail: anda-a@georgikon.hu

[2]*Agricultural Research Institute of the Hungarian Academy of Sciences, Martonvásár, Hungary*

[*]*Corresponding author*

(Manuscript received in final form November 20, 2009)

Abstract—The aim of this analysis is to provide an overview of the precipitation conditions of the Balaton catchments. Because Lake Balaton has shallow water, it responds sensitively to any change in the environment, including precipitation. The influence of the dry period on the lake's water level in the years 2000–2003 serves as a good example for this. Data series of 25 precipitation gauging stations of catchments, recorded between 1921 and 2007, were investigated in this study.. Annual precipitation sums, monthly distribution of rainfall, and the influence of rainfall on natural change in water storage were studied. The whole catchment area was divided into different parts depending on geographical locations and climatic conditions. We found significant differences in the regional precipitation amounts. The western part of the catchments (half of the Zala River basin) has the highest annual precipitation sum, while going towards the east and in the "cut" of the lake, the amount of rainfall decreases. At the majority of the examined stations the decrease in precipitation was also detectable on the basis of WMO climate means, but we did not find explicit decreasing tendencies in the case of several stations. Surface runoff moved collaterally with precipitation decreases, and its impact on natural change in water storage was even more pronounced. The natural change in water storage of the lake is a good indicator reflecting the drying tendency of the recent past, and it calls attention to the necessity of more deliberated water management of the Lake Balaton. Presumably, the precipitation phenomenon, similarly to the past, will also vary in the future. Analysing the data of the past decades may help in making more established decisions.

Key-words: precipitation, Balaton catchments, natural change in water budget

1. Introduction

Investigations of the water budget of Lake Balaton, the largest lake of Central Europe (46°42'6"–47°3'50" N and 17°14'58"–17°14'58" E, its surface is about 600 square kilometers, and the average depth of it is ~3 m) has been ongoing since the 1870s, because of the construction works of the local southern railway. The scientific investigation of the lake (covering gage measurements) was established in the 1890s. However, reliable data series of water budget are available only from the beginning of the 1920s. Besides the most important water supplier of the lake, the river Zala, there are about 50 watercourses. The inflow to the lake is mainly determined by the amount of precipitation. In the last decade, investigations on a local level have been devoted to precipitation depression as a main issue of global warming (*Bartholy et al.*, 2007a; *Kertész* and *Mika*, 1999; *Varga et al.*, 2007). According to the latest PRUDENCE simulations, the annual precipitation sums of Balaton watershed are not expected to change (A2 and B2 scenarios) significantly, but it is not valid to seasonal distribution of rainfall (*Bartholy et al.*, 2009). Decreases in summer precipitation for 2071–2100 are 35% and 20% at A2 and B2 scenarios, respectively. The increase in winter precipitation is the same as the projected rainfall decline in summer. Earlier results of the authors (*Bartholy et al.*, 2001) harmonize with their last projection.

As a result of increased air temperature and precipitation decline, an unprecedented decrease in the water level of the lake was measured around 2000. The former water shortage was restored without any controlled human intervention by the winter of 2003/2004. Similar fluctuations in lake water levels were also observed in other parts of the world (*Gianniou* and *Antopoulos*, 2007; *Mercier et al.*, 2002; *Schindler*, 2001; *Winter et al.*, 2003). Decreases in lake water levels are not independent of global climate change (*Lenters et al.*, 2005). Aspects of climate variability on the lake water level of different sites were reviewed by *Greenland* and *Kittel* (2002).

The most serious problem with handling of Balaton water level is that only reduction of excess water can be controlled, by discharging it through the Sió sluices, but it is not possible to provide a controlled water supply. The inflow to the lake is totally exposed to the precipitation and water amount delivered by surface runoff determined thereby. Any precipitation deficit is immediately reflected by the water level of the lake, like a mirror. *Somlyódi* and *Honti* (2005) projected warmer (0.5–1.5°C) and drier (5–15% less precipitation) climate conditions for Balaton watershed at doubled CO_2 concentration for 2100.

Direction of change in weather of different projections is similar, but the size of change may vary in every scenario. The uncertainty seems to be extremely high regarding the precipitation amount and its distribution.

Antal (1974) determined the multi-year average precipitation amount of the entire watershed as 700 mm in 1951–80. Later it was determined more precisely

broken down to sub-basins; according to this, the source region of Zala River has the most precipitation with an annual amount of more than 800 mm, and the "cut" along the lake proved to be the driest with an annual amount of 700 mm. Above the lake this feature is even less: precipitation of about 600–650 mm is expected. *Varga et al.* (2006) determined the annual average precipitation of 619 mm based on measurements performed between 1921 and 2005. The differing values can be explained by the differences in the period examined. Analysis of the long-term annual precipitation sums shows negative trend (–90 mm/100 year) in more than half of the 17 stations of Hungary. The cited precipitation data were homogenized and controlled by the Hungarian Meteorological Service. Without this thorough check-up, the conclusion will not be adequate for later processing.

The aim of this analysis is to provide an overview of the precipitation conditions of the Balaton catchments for the period from the beginning of reliable precipitation gauging (1921) until the end of 2007. These results are more complex, containing more information than the earlier findings regarding the Balaton watershed or the lakeshore alone (*Béll* and *Takács*, 1974; *Bartholy et al.*, 1995). The Balaton watershed and its surroundings is one of the two most vulnerable regions of Hungary. Although the amount and occurrence of precipitation are important measures, our investigation starts with analysis of monthly and annual precipitation sums. Some of the elements of lake water budget influenced by precipitation were also included in the study. We used the simplest statistical method, the linear trend analysis in our work. This procedure results enough information about the spatial and temporal changes in precipitation amounts. The former precipitation observations generally tried to draw a conclusion from shorter time intervals. The change in precipitation that is analyzed can be utilized in the future for local climate change evaluation of lake's watershed or water budget more precisely.

2. Material and methods

The catchment area of Balaton was divided into five sub-catchments (*Table 1* and *Fig. 1*). Besides geographical position of the sub-catchments, their climate was also taken into consideration. Zala River, the main water supplier, enters the lake on the western side of Balaton, providing 55% of the total water input.

The basin of Zala River was divided into two parts due to the difference in the amount of precipitation. Part I is the western sub-basin of the river, the wettest part of the whole region considered, and includes 6 precipitation gauging stations. The eastern sub-basin of the river is closer to the lake and it is warmer and drier than the western sub-basin. The determination of the remaining three sub-basins was performed on the basis of the former classifications. Parts III–V cover the three corners around the lake: the northern, southern, and eastern sub-basins of Lake Balaton, with 5, 6, and 3 precipitation gauging stations,

respectively. Since the warmest and driest sub-catchment of the region was the eastern one (part V) it was separated from the other sub-regions. As the number of gages was limited on the fifth sub-catchment, outside gages were also included in the study. The largest distance of the outside stations should not exceed 10–15 kilometers from the catchment's border. The precipitation of sub-catchment was equal to the average rainfall measured at different precipitation stations.

Table 1. Main information for sub-catchments of Lake Balaton (* based on Climate Atlas of Hungary, 2002)

Name of sub-catchment areas	Number of stations	Area (km^2)	Annual mean temperature* (°C)	Measured precipitation (mm)	Indicator
River Zala, western	6	1678	9.0– 9.5	650–750	I
River Zala, eastern	5	944	9.5–10.5	630–700	II
Balaton, northern	5	820	9.0–10.5	580–660	III
Balaton, southern	6	1272	10.0–10.5	650–700	IV
Balaton, eastern basin	3	36	10.0–10.5	580–620	V

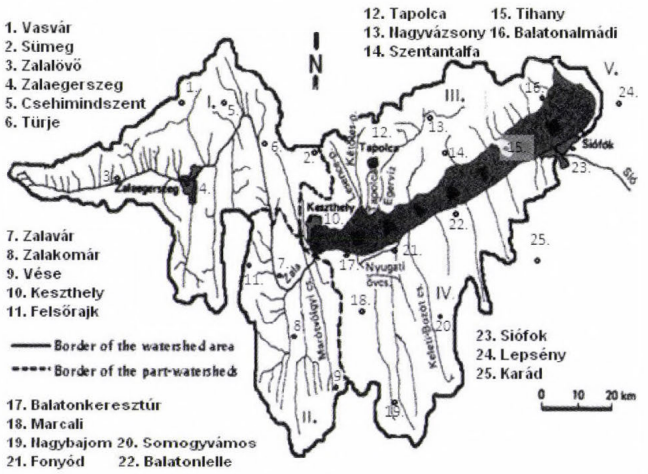

Fig. 1. Catchments of Lake Balaton were divided into five sub-catchments (parts I–V).

The 25 precipitation gauging stations selected for the description of the catchments are part of the precipitation gauging network of the Hungarian Meteorological Service consisting of about 600 stations. At the beginning, gauging stations were equipped exclusively by Hellmann type precipitation gauging units (up to about the middle of the 1990s), that were partly replaced by tipping-bucket automatic devices. The automatic devices were mainly deployed to bigger settlements (Keszthely, Zalaegerszeg, Siófok, Fonyód), and the majority of the stations are still equipped with Hellmann type devices. In the procession,

the monthly and annual amounts were derived from the daily amount of precipitation gaged at 07:00 CET.

Regression analysis of long time series was included in the study. The level of significance referred to in the results was less than 0.05. The critical R^2 value for 87 elements was 0.0446 (linear regression). The statistical evaluation was performed by the free version of STATA 5.0 (1996) program package.

Water budget of Balaton balances the flows in (precipitation, surface water, and groundwater inflows) and out (evaporation, surface and groundwater outflows, surface water withdrawal) of the lake, and the natural change in storage of the lake water (ΔS) is:

$$Inflow - Outflow = \Delta S. \tag{1}$$

In the case of artificially regulated lakes as Lake Balaton, the change in natural water storage is

$$\Delta S = (P + I) - E, \tag{2}$$

where P is the precipitation (mm), I is the surface runoff (mm), and E is the evaporation (mm). Change in water storage represents modification in the lake water level. To characterize S, the lake evaporation (E in mm) was calculated by using the classical Meyer formula between 1921 and 1985. Regarding the relatively large error in evaporation estimates, the so-called Balaton formula was introduced after 1985 (*Antal*, 1963). Partial analysis of evaporation was excluded from the study.

The surface runoff was calculated statistically by using the measured discharge of principle streams. More details can be found in *Varga* (1986).

3. Results and discussion

3.1. The annual amount of precipitation over the Balaton catchments

According to the PRUDENCE results for 2071–2100, regional warming with a mean temperature rise of 3.2–4°C is projected in the Carpathian Basin (*Bartholy et al.*, 2009). It is expected that drying will not be even and will be concentrated in the summertime (25–35% decline in the amount of rainfall). In our investigation we reviewed the changes that have already occurred in the amount of precipitation first; for other experts it can serve as a good starting point for establishing future scenarios. Future precipitation prognosis is excluded from our study.

The regional average of the annual precipitation amount calculated for the entire catchment based on the data of the 25 stations for the period of 1921–2007 is 684.4 ± 111.4 mm. The year with the highest amount of precipitation was 1965 with 986 mm. The driest year of the observed period was 2000, with 458 mm. These two extreme values well demonstrate the eccentric precipitation

regime of the Carpathian Basin, where the ever measured wettest year may gain three times more precipitation than the driest year.

In spite of consistent negative signs in the regression coefficient of annual precipitation sums, the decline was not always significant at every station. We found a significant decrease in annual precipitation sum (that covered several stations) only in the case of the western sub-catchments of Zala River (part I), where a drop in precipitation (1.1–1.7 mm in annual average) was justifiable during the period from the beginning of gauging to date in the case of four out of six stations (*Table 2*). For the whole investigation period it means 95–146 mm precipitation depression depending on the place of the station. The confidence intervals in *Table 2* have got meaning only when the rainfall change is significant. Values of regression coefficient have to fall in the confidence intervals on 95% probability level.

Table 2. Development of the annual sums of precipitation at stations for 1921–2007. Stations showing significant changes in rainfall are in bold (*station excluded from the watershed)

Station	Regression coefficient (mm/year)	R^2	Confidence intervals	
			Lower	Upper
Vasvár	–0.056	0.000	–1.0902	0.9796
Sümeg	**–1.128**	**0.048**	**–2.2087**	**–0.0477**
Zalalövő	**–1.336**	**0.048**	**–2.6217**	**–0.0519**
Zalaegerszeg	**–1.736**	**0.109**	**–2.8066**	**–0.6668**
Csehmindszent	–1.004	0.039	–2.0752	0.0671
Türje	**–1.103**	**0.050**	**–2.1354**	**–0.0692**
Zalavár	–0.942	0.029	–1.9491	0.257
Zalakomár	–0.771	0.018	–1.9884	0.4457
Vése	–1.049	0.028	–2.3673	0.0269
Keszthely	**–1.480**	**0.073**	**–2.6127**	**–0.3471**
Felsőrajk	–1.020	0.033	–2.2161	0.1753
Tapolca	–0.967	0.037	–2.0257	0.0899
Nagyvázsony	**–1.323**	**0.066**	**–2.3976**	**–0.2493**
Szentantalfa	–0.303	0.003	–1.3639	0.7578
Tihany	–0.787	0.028	–1.7765	0.2019
Balatonalmádi	–0.944	0.038	–1.9609	0.072
Balatonkeresztúr	–0.655	0.015	–1.7728	0.4612
Marcali	–0.071	0.000	–1.3556	1.2141
Nagybajom	–0.383	0.004	–1.6584	0.8908
Somogyvámos	–0.867	0.025	–2.0338	0.3009
Fonyód	**–1.385**	**0.054**	**–2.6252**	**–0.1453**
Balatonlelle	–0.020	0.000	–1.0081	0.9651
Siófok	**–1.404**	**0.087**	**–2.3817**	**–0.4276**
Lepsény*	–0.47	0.010	–1.4403	0.4989
Karád*	–0.392	0.005	–1.5305	0.7469

In the case of the other four sub-catchments (though the regression coefficients of the trend lines are negative), we found a significant decrease in the annual amount of precipitation time series at one station from each (Siófok, Fonyód, Nagyvázsony, Keszthely). At the majority of the stations, in the case of three out of four sub-catchments showing changes in precipitation that cannot be statistically justified – in an interesting way – the only gauging location showing significant decrease was at the lakeshore (Keszthely, Fonyód, and Siófok).

The average rate of precipitation decline computed from the regression coefficients for the whole watershed is 86 mm/100 year. Previous work on precipitation trend of whole Hungary (*Koflanovits-Adámy* and *Szentimrey*, 1986) for the time period of 1901–1984 provided almost the same result (–90 mm/100 year). It is interesting that decline in precipitation of the past two decades did not influenced strongly the regression coefficient. The possible reason might have been the yearly precipitation sums used as a basis in this study.

On the basis of the recommendation of the WMO, we created 10-year running climate norms (*Fig. 2*). In *Fig. 2*, the decreasing precipitation characteristic of the majority of the stations is demonstrated by the data of Zalaegerszeg station located at the centre of the catchments (sub-catchments I) (*Fig. 2a*). All the other sub-figures contain the exceptions. The constant amount of rainfall for Tihany compared to the other stations is remarkable; it is in connection with the geographical location of the gauging station. Tihany is located on the only peninsula pushing out into the lake (*Fig. 2b*). The relatively less yearly amount of rainfall in Tihany is closer to the lower amount of precipitation falling to the lake surface.

The amount of precipitation measured at the other stations show fairly diversified pictures in time, but at 21 out of 25 stations the period between 1921 and 1970 was wetter, followed by a drying period. The abovementioned tendency did not emerge at four stations; 3 of them are located in the southern river basin of Lake Balaton (Balatonlelle, Marcali, and Nagybajom); here there was a modest increase in precipitation in the period up to 1970, then came the decrease lasting up to the present (*Figs. 2c–e*).

There were only three out of the 25 precipitation gauging stations (Marcali, Zalalövő, and Csehimindszent) where the last two climate norms (the period between 1971 and 2007) were not the two driest ones (*Figs. 2d–g*). Looking for the reasons we did not find any change in location or environmental conditions of the stations. The amount of rainfall slightly increased until the 1960s, and from the 1980s to present a decreased tendency manifested. Our multi-year precipitation data for the largest part of the Lake Balaton catchments correspond well to the studies demonstrating this drying tendency of the last decades (*Bartholy et al.*, 2007b; *Kertész* and *Mika*, 1999; *Nováky*, 1991).

The mean rate of precipitation decline for the whole watershed is 83.4 mm/-100 year (*Fig. 3*). Until now, the decrease was not significant at less than 0.05 significance level.

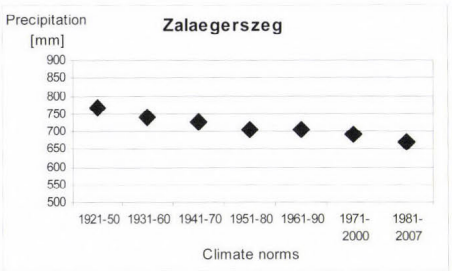

(a)

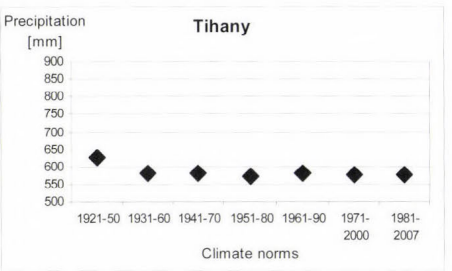

(b)

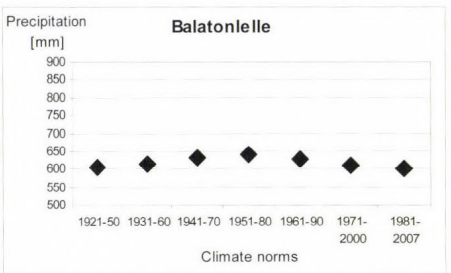

(b)

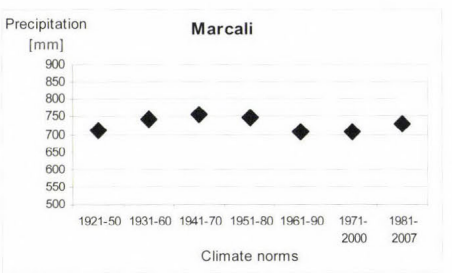

(d)

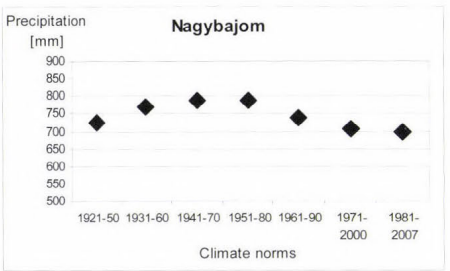

(e)

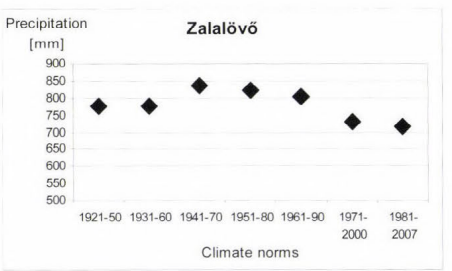

(f)

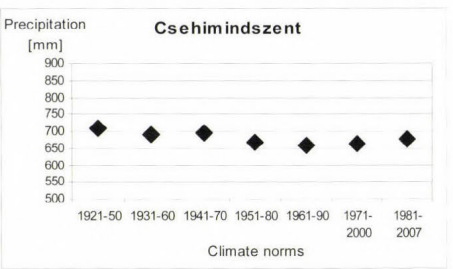

(g)

Fig. 2. Mean annual precipitation sum for 30-year-long time periods at some selected stations of the Balaton catchment area

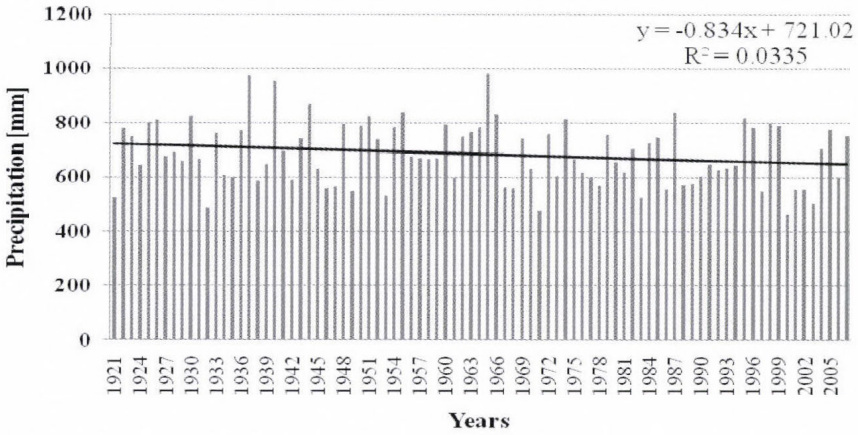

Fig. 3. Variation in yearly precipitation sums for the Balaton catchments (1921–2007)

From the point of view of the development of the lake's water budget, the annual distribution of precipitation is also important. Earlier studies pointed out two maximum points in the annual variation of monthly precipitation sums in the catchments of the lake (*Bartholy et al.*, 2001). The main maximum point is the consequence of wet air inflowing from the Atlantic Ocean at the beginning of summer. The second maximum point is in October-November, owing to the intensifying cyclone activity coming from the Mediterranean basin (*Antal*, 1974). Several studies analyzing Hungary's precipitation conditions found moderate spatial and temporal shift in annual distribution of rainfall sums (*Ambrózy et al.*, 1990). Less than 10% change was observed in the southwestern region of the country, like in the area of the Balaton catchment. *Bartholy et al.* (1995) published that the modification in annual rainfall distribution is one of the local consequences of global warming. Significant decrease in the second peak of precipitation amounts was not confirmed by the precipitation data of the 25 stations located in the catchments of Lake Balaton. On the contrary, in the case of 10 out of the 25 stations (Sümeg, Zalavár, Zalakomár, Vése, Tapolca, Balatonkeresztúr, Marcali, Fonyód, Balatonlelle, Siófok), the ratio of precipitation in August has risen significantly, by 5–10%, compared to the main maximum point in the past 30 years. The uncertainty of the precipitation in the winter months and the higher variability of the amount of precipitation can be experienced. Our observations correspond to the outcomes published to Balaton watershed by *Bartholy et al.* (1995) and *Varga et al.* (2004).

3.2. Water budget elements closely related to precipitation: surface runoff and release through the Sió sluices

Among the two referred elements, the release is intensively affected not only by the rainfall, but by the amount of evaporation. The aim of our investigation was

the study of precipitation and strongly concerned elements as surface runoff and release in the vicinity of Lake Balaton. Knowing the importance of evaporation in lake water budget, we took it into account where it was necessary, but we did not focus on it, discussion of evaporation is excluded from this work.

Watercourses deliver the larger part (about 60%) of the entire lake water acquisition. In the period studied, the annual average surface runoff was 873.9 ± 300 mm (*Fig. 4*) with the maximum of 1974 mm measured in 1965, and the minimum of 293 mm determined both in 2002 and 2003. There were 26 out of 87 years of the whole time series (about one-third) when the surface runoff exceeded 1000 mm, and only two of them were after the year 2000 (dry spell). The average runoff fell back to 501 mm in 2000 and remained on this value until 2004. The moderate decrease in precipitation leads to higher depression in surface runoff. Even in the case of non-significant precipitation changes, 42.7% reduction in runoff seriously affected the lake water level in the beginning of the 2000s. Recovery of the lake water level was late. This is in contrast with other semi-arid regions, where surplus water after drought is mostly used for infiltration and replenishment of groundwater resources, and the surface runoff to the stream-network appears only at a later stage (*Varga et al.*, 2007). The authors mentioned that despite the humid years of 2004 and 2005, the runoff depression still was one third of the average.

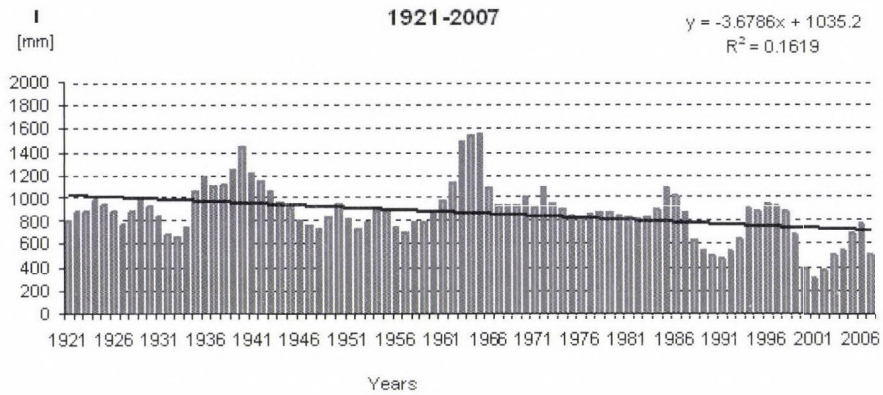

Fig. 4. Annual variation in inflow (*I* mm) for the investigation period (based on data provided by the VITUKI). The change is significant at less than 0.05 significance level.

Signs of change in the annual variation of surface runoff were the same as for precipitation, and water depression was even significant at less than 0.05 significance level. From the beginning of measurements (1921) to the present, the surface runoff has fallen by 315.6 mm (*Fig. 4*). Similar results were published by *Nováky* (1991).

Because of the precipitation pattern and crop cover modifications in Hungary, the runoff has special seasonal variability (*Table 3*).

Table 3. Monthly averages of runoff in the Balaton region. Months having significant change below the 0.05 significance level are in bold

Month	Average runoff (mm/month)	Direction of change	Degree of change (mm/year)
January	81.6	not changed	0.008
February	**99.2**	**decreasing**	**–0.481**
March	121.1	not changed	–0.637
April	96.4	not changed	–0.297
May	**74.5**	**decreasing**	**–0.312**
June	**64.4**	**decreasing**	**–0.411**
July	**54.7**	**decreasing**	**–0.400**
August	44.7	not changed	–0.222
September	43.0	not changed	–0.126
October	49.6	not changed	–0.092
November	66.7	not changed	–0.037
December	78.0	not changed	0.044

The highest values are observed in early spring (February, March, and April). In winter time, there is an increase in the development of surface runoff. Out of the monthly figures of the decrease in water input caused by runoff, the following decreases were significant: at the end of winter in February, then from the end of spring in May, June, and July. The phenomenon experienced in this latter period is doubly dangerous; first, the statistically justified failure in lake water input occurred in summer, in the hottest period with the highest evaporation level; second, the amount of water coming from the catchments and feeding the lake fell back in several subsequent months.

The release of excess water through the Sió sluices is the only water budget member that is a result of controlled human intervention. The aim is to control the lake water level that is regulated by actual law whose borders are not constant in time. The desired level of Lake Balaton is between 0.7 and 1.1 m regulated in 1997 for the last time.

Because of precipitation deficit and surface runoff depression, the quantity of release dropped drastically in the past decade (*Fig. 5*). During the drought of 2000–2003, the Sió sluices were closed, but in 2006 and 2007 they were opened again. Note, that there is an other important affecting factor, the evaporation, but since this is not directly influenced by the precipitation, it is excluded from this study.

Cumulative precipitation and surface runoff shortage were the causes of the change of sign in natural water storage from positive into negative from 2000 to 2003 (*Fig. 6*). During this unique dry period, the water input was not enough to

cover the water necessity of lake evaporation. This negative phenomenon left a mark on ΔS as well. The most variable indicator of Lake Balaton is change in natural water storage, whose average is 592.8 ± 400 mm. Its highest value reached 2031 mm in 1965, and the lowest one was only –180 mm in 2003. The cumulative water deficit of the lake broke the record between 2000 and 2004.

Analysis of the annual variation in ΔS statistically proves a decreasing tendency at less than 0.05 significance level (389.9 mm/100 years). Similarly to the other factors at the input side of the lake water budget, the values of the past two decades falling behind average are worrisome.

Decline in natural change in water storage is more pronounced during summer. In most cases the ΔS increased in winter.

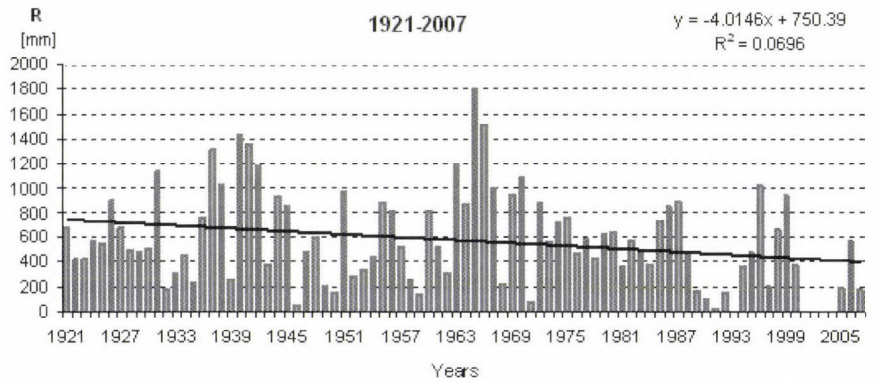

Fig. 5. Annual variation in release (R mm) through the Sió sluices from 1921 until present (based on data provided by the VITUKI).

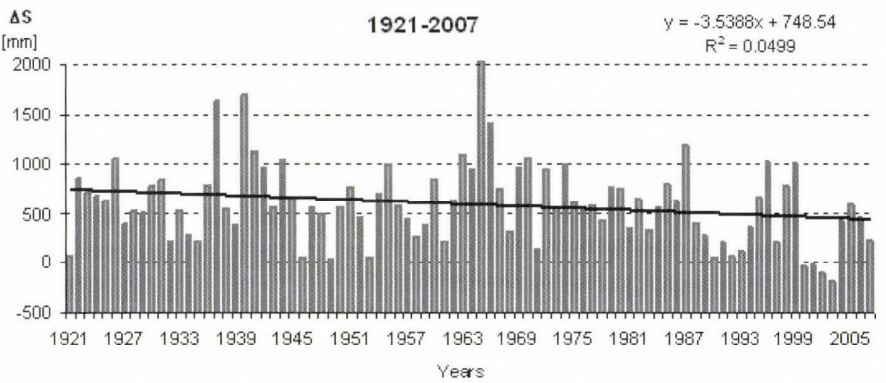

Fig. 6. Natural change in water storage (ΔS mm) from the beginning of the investigation period ((based on data provided by the VITUKI)). The change is significant at less than 0.05 significance level.

4. Conclusions

In the period between 1921 and 2007, the annual precipitation showed a decreasing tendency in the catchments of Lake Balaton, though this change could only be significantly justified in the western part of the basin of Zala River and at several stations close to the lakeshore. At the same time the western side of Zala River is the wettest part of the whole catchments regarding the annual amounts of rainfall. The statistically justifiable decrease in precipitation of the lakeshore stations of the other sub-catchments renders lesser danger, since these contribute to the surface runoff to a smaller extent, and the occurrence of less, and less "disturbing" precipitation is unanimously positive for the bathing holiday-makers.

Distribution of precipitation has not significantly changed at the 25 stations of the lake's catchments. Examining a longer time period, the two maximum points can still be followed. It is a positive phenomenon that a 5–10% rise in the precipitation of August can be experienced. This event is beneficial, since this is the period when the intensified evaporation owing to the higher summer temperature can seriously decrease the water level.

An unfavorable sign considering the water level of the lake is that the runoff has significantly decreased, mainly in the past two decades. In the decades before 1990, the runoff seemed to be a more stable element based on yearly means. The reduction of the lake's water inflow was compensated by the reduction of release in the period after the 1990s. Release through the Sió sluices is the only controlled factor to regulate the water level of Lake Balaton. Similarly to the reduction of inflow, release has also decreased over the past several decades. This human intervention should be implemented with special care, mainly with the knowledge of the reduced amount of inflow during the summer months.

A good example of the local variability caused by global climate change is the annual rainfall sum recorded at various meteorological stations in the watershed of Lake Balaton. The most sensitive region of the watershed is the western part containing the river Zala, where, although the mean drop in annual rainfall quantity since 1921 was only 1.5 mm, the annual decrease in runoff, which is also influenced by rainfall, was more than twice as great. Earlier observations suggest that this is especially dangerous, because when wet years follow dry periods, the infiltration and replenishment of groundwater resources causes a further delay in the runoff (*Varga et al.*, 2007). One positive observation is that, despite the decline in mean annual rainfall over the last 30 years, a 10–15% increase in monthly precipitation has been noted in August at most stations. This could compensate the water supplies of the lake to some extent for the increased evaporation experienced during the summer months.

Greater changes in the rainfall sums recorded at the various stations were observed at stations situated in the immediate vicinity of the lake (Keszthely,

Siófok, Fonyód). This is important, because these are the most frequented regions of the watershed, and thus, they are the most exposed to environmental load. This should be emphasized when compiling long-term land-use plans.

Acknowledgement—We express our gratitude to colleagues of the Central-Transdanubian Environmental and Water Authority (VITUKI), especially *György Varga*, for providing data used in this analysis.

References

Ambrózy, P., Koflanovits, E. and *Kövér, B.*, 1990: Shift in temporal distribution of precipitation amounts in Hungary (in Hungarian). *Időjárás 94*, 156-167.

Antal, E., 1974: Characterisation of the members of heat and water balances in Balaton region. In *The Climate of Balaton* (eds.: *B. Béll* and *L. Takács*) (in Hungarian). Országos Meteorológiai Intézet, Budapest, 188-204.

Antal, E., 1963: Evaporation of Lake Balaton (in Hungarian). *Időjárás 67*, 290-297.

Bartholy, J., Pongrácz, R., Gelybó, Gy. and *Szabó, P.*, 2009: Analysis of expected climate change in the Carpathian Basin using the PRUDENCE results. *Időjárás 112*, 249-265.

Bartholy, J., Pongrácz, R. and *Gelybó, Gy.*, 2007a: Regional climate change expected in Hungary 2071–2100. *Applied Ecol and Environ Res 5*, 1-17.

Bartholy, J. and *Pongrácz, R.*, 2007b: Regional analysis of extreme temperature and precipitation indices for the Carpathian Basin from 1946 to 2001. *Global Planet Change 57*, 83-95.

Bartholy, J., Matyasovszky, I. and *Weidinger, T.*, 2001: Regional climate change in Hungary: a survey and stohastic downscaling method. *Időjárás 105*, 1-17.

Bartholy, J., Bogárdi, I. and *Matyasovszky, I.*, 1995: Effects of climate change on regional precipitation in Lake Balaton watershed. *Theor Appl Climatol 51*, 237-250.

Climate Atlas of Hungary (in Hungarian), 2002, Országos Meteorológiai Szolgálat, Budapest.

Gianniou, S.K. and *Antonopoulos, V.Z.*, 2007: Evaporation and energy budget in Lake Vegoritis, Greece. *J Hydrol 345*, 212-223.

Greenland, D. and *Kittel, T.G.F.*, 2002: Temporal variability of climate at US Long-Term Ecological Research (LTER) sites. *Climat Res 19*, 213-231.

Kertész, A. and *Mika, J.*, 1999: Climate Change in South-Eastern Europe. *Phys Chem Earth (A) 24*, 913-920.

Koflanovits-Adámy, E. and *Szentimrey, T.*, 1986: The variations of precipitation amounts in the Carpathian Basin during the present century (in Hungarian). *Időjárás 90*, 206-216.

Lenters, J.D., Kratz, T.K. and *Bowser, C.J.*, 2005: Effects of climate variability on lake evaporation: Result from a long term energy budget study of Sparkling Lake, northern Wisconsin (USA). *J Hydrol 308*, 168-195.

Mercier, F., Cazenave, A. and *Maheu, C.*, 2002: Interannual lake level fluctuations (1993–1999) in Africa from Topex/Poseidon connections with ocean-atmosphere interactions over the Indian Ocean. *Global Planet Change 32*, 141-163.

Nováky, B., 1991: Climate effects on runoff conditions in Hungary. *Earth Surface and Landforms 16*, 593-601.

Schindler, D.W., 2001: The cumulative effects of climate warming and other human stresses on Canadian freshwaters in the new millenium. *Can J Fish Aquat Sci 58*, 18-29.

Somlyódi, L. and *Honti, M.*, 2005: The water substitution of Lake Balaton (in Hungarian). *Magyar Tudomány 5*, 570-581.

STATA 5.0, 1996: Stata Corporation LP Texas, USA, www.stata.com

Varga, Gy., 1986: Developing calculation of water budget of Lake Balaton (in Hungarian). *Report on Research carried out on Lake Balaton by VITUKI*, Budapest.

Varga, Gy., Papp, U.J. and *Bálint, G.*, 2007: Recent extremes in the water budget of Lake Balaton. *Georgikon for Agric 10*, 25-40.

Varga, B., Boldizsár, A. and *Gimesi, L.*, 2006: Some remarks on water balance components of Lake Balaton. *Georgikon for Agric 10*, 69-82.

Varga, Gy., Papp, U.J., Mika, J., Pálfy, L. and *Bálint, G.*, 2004: The 2000–2003 extremes in the water budget of Lake Balaton. *Geophys Res Abstract Vol. 6 07795*, SRef-ID: 1607-7962/gra/EGU04-A-07795.

Winter, T.C., Buso, D.C., Rosenberry, D.O., Likens, G.E., Sturrock, A.M. and *Mau, D.P.*, 2003: Evaporation determined by the energy budget method for Mirror Lake, New Hampshire. *Limnol Oceanogr 48*, 995-1009.

IDŐJÁRÁS

Quarterly Journal of the Hungarian Meteorological Service
Vol. 114, No. 3, July–September 2010, pp. 203–215

Surface resistance estimation of some crops using different climate, soil-, and vegetation-specific data

Hajnalka Breuer and **Ferenc Ács**

Department of Meteorology, Eötvös Loránd University
P.O. Box 32, H-1518 Budapest, Hungary;
E-mails: bhajni@nimbus.elte.hu, acs@caesar.elte.hu

(Manuscript received in final form May 25, 2010)

Abstract — Annual course of different crop surface resistance (r_c) parameters at Szarvas was analyzed. In the analysis, a set of independent climatological, satellite, soil- and vegetation-specific data was used. Soil- and plant-specific data were taken from the literature. Of plant-specific data, the plant coefficient data determined by evapotranspirometer measurements were used. The soil texture at Szarvas is clay. The estimation method of r_c is based on calculating the ratio between the actual and potential evapotranspiration, which is a proven method for climatological applications.

It is found that r_c is mainly governed by the changes of the available water in the soil. It is also found that r_c variations induced by variations of the available water in the soil are much larger than r_c variations induced by plant species changes represented by plant coefficients. The analysis showed that some results obtained in the faraway past can also be successfully used for "state of the art" biophysical modeling purposes in the meteorology.

Key-words: climate data, soil data, evapotranspirometer measurements, plant coefficients, actual and potential evapotranspiration, crops, surface resistance

1. Introduction

The first evapotranspirometer measurements in Hungary started in the 1960s. Daily potential evapotranspiration was measured using Thornthwaite-Mather evapotranspirometers (*Thornthwaite* and *Mather*, 1955) above different vegetation types like short grass, potato, apple, winter wheat, and corn to work out irrigation scheduling for each vegetation type separately. The first description and user guide of this apparatus in Hungary was given by *Antal* (1966). These measurements served agrometeorological goals. It should be mentioned that Thornthwaite's scientific influence in Hungary was strong; this could be seen not only via using Thornthwaite's type evapotranspirometer (e.g., *Antal*, 1968;

Posza and *Stollár*, 1983) but also via application of Thornthwaite's climate classification system (*Szesztay*, 1958; *Kakas*, 1960).

In about the same period, the first mesoscale modeling systems were applied (*Deardorff*, 1977, 1978). These models contain complex biophysical modules for simulating exchange processes at the interface between the land surface and the atmosphere. The exchange processes could be described only by characterizing albedo, roughness length, and the surface resistance of the soil-vegetation system. Albedo is the most important radiation transfer parameter. Roughness length parameter determines strongly the intensity of the turbulent transfer. Surface resistance (r_c) is a basic parameter for characterizing water transfer in the soil-vegetation system which was introduced by *Monteith* (1965) analyzing the process of evapotranspiration from vegetated surfaces. Of the three parameters mentioned, the latter one is the most changeable, so the uncertainties related to it are also the largest.

In this study, we will focus on the estimation of r_c of some chosen crops which are common in Hungary. r_c is estimated using a common climatological method based on calculation of the ratio between the actual and potential evapotranspiration. The aim of this study is to determine and analyze the annual course of r_c of some chosen crops at Szarvas using the above mentioned method. The analysis was performed using plant coefficient data obtained from evapotranspirometer measurement results (*Antal*, 1968; *Posza* and *Stollár*, 1983) and some other needed environmental data (*Mitchell et al.*, 2004; *Bartholy et al.*, 2004). All data refer to Szarvas, but they are representative for different time periods. This shortcoming is less important in the case of climatological analysis. The novelty of the study does not lie in the methodology applied but rather in the combination of the data which will be presented below. It should be mentioned that, to the best of our knowledge, there is not any study in Hungary in which r_c would have been analyzed from either meteorological or climatological point of view.

2. Data

Climate and soil data are used in this study. Climate data can be classified into three groups: meteorological data, satellite data, and in-situ vegetation specific data obtained by using evapotranspirometer measurements.

2.1. Meteorological and satellite data

Mean monthly precipitation (P), air temperature (T), and diurnal temperature range data constitute meteorological data. They were taken from the CRU (**C**limate **R**esearch **U**nit), which is one of the well-known climate data centers. The CRU TS 1.2 (*Mitchell et al.*, 2004) database contains four observed state variables and one parameter (2 m air temperature, diurnal temperature range,

precipitation, cloud cover, and vapor pressure) interpolated to a 10' (≈ 11 km) resolution grid over Europe from 1901 to 2000 on a monthly scale. The interpolation was made using the measurements of meteorological stations in Europe. Naturally the accuracy of the fields is increasing in time, as the number of measurements is increasing. The spatial resolution is high enough to be taken as a reference measurement field used for verification and validation of climate models. From this database the nearest point to Szarvas was taken, which is only 0.02° away.

Satellite measurement of ten-day composite *NDVI* (normalized difference vegetation index) data (*Bartholy et al.*, 2004) is freely available from 1982 up to 2000 at a 8 km horizontal resolution from the NASA Goddard Space Flight Center. Naturally, we could not acquire such data to 1960 as there were not any kind of measurements of *NDVI*. For our purposes, we calculated the average *NDVI* of the 1982–2000 period for Szarvas. These data together with *P* and *T* are presented in *Table 1*.

Table 1. Monthly mean values of *NDVI*, *T*, and *P* referring to period 1982–2000 as used for Szarvas

Month	*NDVI*	*T* (°C)	*P* (mm)
January	0.147	–0.866	27.544
February	0.160	1.097	30.823
March	0.231	5.789	24.359
April	0.412	11.995	47.269
May	0.547	17.038	58.081
June	0.507	20.055	64.794
July	0.441	22.005	49.754
August	0.401	21.745	45.933
September	0.346	17.395	43.840
October	0.298	11.986	35.553
November	0.262	5.506	43.594
December	0.157	0.714	41.877

2.2. Plant coefficients

In this study, five-day average plant coefficient values (*b*), published by *Posza* and *Stollár* (1983), were used. Seasonal changes of the values of *b* for different plant species are presented in *Fig. 1*. The values were obtained by using measurement results of Thornthwaite-Mather's circular evapotranspirometers (surface equals to 4 m^2, depth is 70 cm), in which the level of water was kept 40 cm below the surface by an automatic level control. The measurements were performed at different locations in Hungary, but mostly in Szarvas. The time interval of the measurements was different for different vegetation types. It is to

be noted that important details concerning the measurements were described by *Antal* (1968) and *Posza* and *Stollár* (1983). Inspecting *Fig. 1*, some interesting features could be noted. Values of the *b* coefficient referring to grass show a step-like change; this is caused by its systematic cutting. It could also be seen that the growing season of winter wheat lasts until the middle of July. This could be true, but only under measurement conditions which insured always sufficient water. So, values of *b* for winter wheat in July do not reflect the real state of winter wheat which prevails on the ploughlands. The same is valid for the *b* values of apple at the end of October. It is obvious that the *b* values obtained refer to the conditions when the water supply is good.

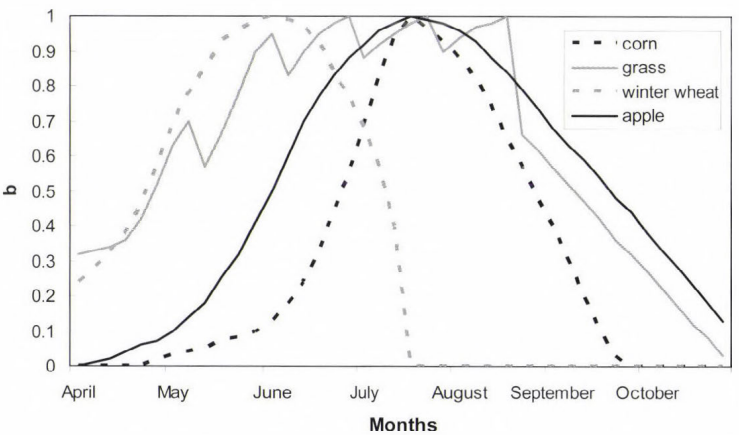

Fig. 1. Seasonal changes of plant coefficients for different plant species as reported by *Posza* and *Stollár* (1983). Monthly values are obtained by using five-day averages.

2.3. Soil data

For calculating actual evapotranspiration, soil data are also needed. At Szarvas, clay is the prevailing soil texture (*Várallyay et al.*, 1980). The most important soil hydraulic parameters of this soil texture are presented in *Table 2*. The values presented were obtained using the results of *Nemes* (2003) and *Fodor* and *Rajkai* (2005).

Table 2. Soil hydrophysical properties used in calculation (saturated, field capacity, and wilting point soil water contents, Θ_s, Θ_f, Θ_w, respectively; Clapp-Hornberger pore size index, b_{CH}; saturated soil water conductivity, K_s)

Θ_s (mm m^{-1})	Θ_f (mm m^{-1})	Θ_w (mm m^{-1})	b_{CH}	K_s (m s^{-1})
527.94	469.55	140.24	6.15	$8 \cdot 10^{-7}$

3. Method

3.1. Basic equation

The ratio of actual (E) and potential (E_p) evapotranspiration (often noted as β) using Penman-Montieth's equation (*Monteith*, 1965) can be expressed as

$$\beta = \frac{E}{E_p} = \frac{\Delta + \gamma}{\Delta + \gamma(1 + r_c / r_a)}, \tag{1}$$

where Δ is the slope of the saturated vapor pressure versus air temperature T, γ is the psychrometric constant (0.65 hPa K^{-1} value is used in this study), r_c is the surface resistance of the soil-vegetation system, and r_a is the aerodynamic resistance characterizing turbulent transfer above the soil-vegetation system.

β can also be expressed by using an empirical formula. *Antal* (1968) presents a formula based on Thornthwaite-Mather's evapotranspirometer measurements:

$$\beta_{hun} = \frac{F_{ma} + b}{1 + b} F_{ma}, \tag{2}$$

where $F_{ma} = (\Theta - \Theta_w)/(\Theta_f - \Theta_w)$, Θ is the actual soil moisture content [$m^3\ m^{-3}$], Θ_f is the field capacity soil moisture content [$m^3\ m^{-3}$], Θ_w is the wilting point soil moisture content [$m^3\ m^{-3}$], and b is the plant coefficient (*Posza* and *Stollár*, 1983). Since the b values obtained refer to the conditions when the water supply is good the formula of *Antal* (1968) is more suitable for describing evapotranspiration in wet than in dry conditions.

Equating Eqs. (1) and (2), it is easy to obtain an expression for r_c:

$$r_c = \frac{1 - \beta_{hun}}{\beta_{hun}} \frac{\Delta + \gamma}{\gamma} r_a. \tag{3}$$

According to *Szeicz* and *Long* (1969), Eq. (3) is suitable for estimating monthly values of r_c in the growing season when monthly values of r_a are available. This opinion can be accepted knowing that the relationship between the stomata and the near surface atmosphere is the strongest when unstable stratification is prevailing (*Jarvis* and *McNaughton*, 1986; *Ács*, 2008; *Breuer*, 2009). Since during evapotranspirometer measurements there were no measurements for determining r_a, the range of the changes of r_a has to be estimated after some assumptions regarding climatic (wind) conditions and vegetation morphology (roughness length) characteristics. We supposed that the wind speed varies mainly between 1–4 $m\ s^{-1}$ in the growing season and that the roughness length

of the investigated plant species changes between 0–0.4 m. For above mentioned conditions, the typical values of r_a in unstable stratification vary between about 5–50 s m^{-1}. The lowest values refer to apple (large roughness), while the highest values refer to grass (small roughness). For stable stratification, the r_c *versus* r_a relationship is weak and it becomes always weaker with the growing atmospheric stability (*Ács*, 2008), therefore, Eq. (3) cannot be applied for these conditions at all. It is to be mentioned, that these considerations refer only to vegetation, namely, the bare soil surface resistance does not depend upon r_a at all.

3.2. Estimating of soil moisture content and leaf area index

For estimating r_c, it is necessary to calculate Θ. Θ was calculated by using a 1 m deep bucket type model. The potential evapotranspiration (*PET*) was calculated after *Turc* (1961). The radiation in Turc's formula was estimated by using Hargreaves expression (*Hargreaves* and *Samani*, 1982). Using F_{ma}, the partitioning of the *PET* to the actual evapotranspiration (*AET*) was calculated. The model estimates water deficiency and surplus from *P* and *AET*. An estimation of gravitational runoff (*Clapp* and *Hornberger*, 1978) was also incorporated.

For estimating the minimum stomatal resistance parameter (r_{stmin}), it is necessary to know the leaf area index (*LAI*) values. There are many methods for estimating *LAI*; we used a formula which is based on normalized difference vegetation index (*NDVI*) estimations. According to *Zhangshi* and *Williams* (1997),

$$LAI_i = LAI_{\max} \frac{NDVI_i - NDVI_{\min}}{NDVI_{\max} - NDVI_{\min}}, \tag{4}$$

where max, min, and *i* subscripts denote maximum, minimum, and actual values, respectively. The *NDVI* values represent observed values. The formula assumes that *NDVI*/*LAI* relationship is linear (*Wiegand et al.*, 1979; *Wardley* and *Curran*, 1984); and that the maximum *NDVI* value in a season correspond to the maximum *LAI* of vegetation cover (*Justice*, 1986). This latter fact does not mean that $LAI_{\max}$ has to be determined by all means from $NDVI_{\max}$; this could also be achieved using independent sources.

4. Results

The results obtained will be analyzed in three steps. First, the β_{hun} values shall be considered. After this, an analysis of r_c will be given. Lastly, we shall try to give an estimate for r_{stmin} because of its importance in the mesoscale models. We will show that this is possible only if enough accurate *LAI* values are available.

4.1. Monthly values of β_{hun}

β_{hun} represents the ratio between the actual and potential evapotranspiration. It is parameterized after *Antal* (1968), (Eq. 2); it depends upon F_{ma} and b. Note that F_{ma} is estimated using a bucket type model, while b is taken from *Posza* and *Stollár* (1983). When no b values were available, for instance, in the time period after growing season, then the b values used were put to zero. Seasonal changes of β_{hun} are presented in *Fig. 2*. β_{hun} is plotted as the plant species mean (β^{mean}_{hun}) and for all plant species separately. It has to be said that β_{hun} refers to Szarvas though b values of some plant species (for instance apple) were determined by performing evapotranspirometer measurements outside Szarvas. It is essential, that the course of F_{ma} and β_{hun} is very similar. There is a maximum in March and a minimum in September or October. The variability of β_{hun} according to plant species is observable. Nevertheless, the largest β_{hun} differences caused by b differences are as large as the standard deviation of β^{mean}_{hun}. This difference is the largest between the apple and winter wheat in the middle of August. It should be underlined that β_{hun} variations caused by b differences are equivocally smaller than those β_{hun} changes which were caused by F_{ma} changes.

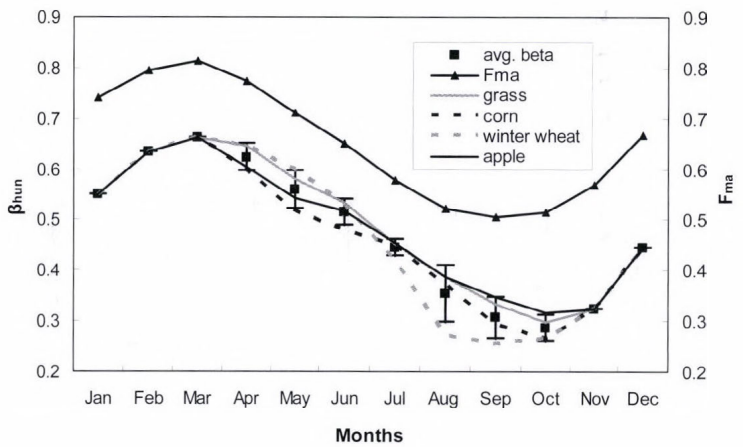

Fig. 2. Annual course of relative water-holding capacity (F_{ma}) and the ratio between the actual and potential evapotranspiration (β_{hun}) for different plant species.

4.2. Monthly values of the land-surface resistance

Land-surface resistance (r_c) is a weighted mean of soil and vegetation canopy resistances. For closed vegetation canopy, r_c converges to the canopy resistance. According to the model (Eq. 3), r_c depends upon β_{hun}, air temperature (via Δ), and atmospheric stratification (via r_a). Note that there is a linear dependence between the r_c and r_a, though in reality r_c is weakly and indirectly dependent

upon atmospheric stratification. This could be checked by using those models, where r_c is parameterized as a function of leaf water potential (*Ács*, 1994; *Ács* and *Hantel*, 1998). Despite its former weakness, Eq. (3) could be successfully used for determining r_c if it serves climatological purposes, for instance, when a long series of evapotranspiration measurements are available (*Szeicz* and *Long*, 1969). Dependence between r_c and r_a for different plant species and months is presented in *Fig. 3*.

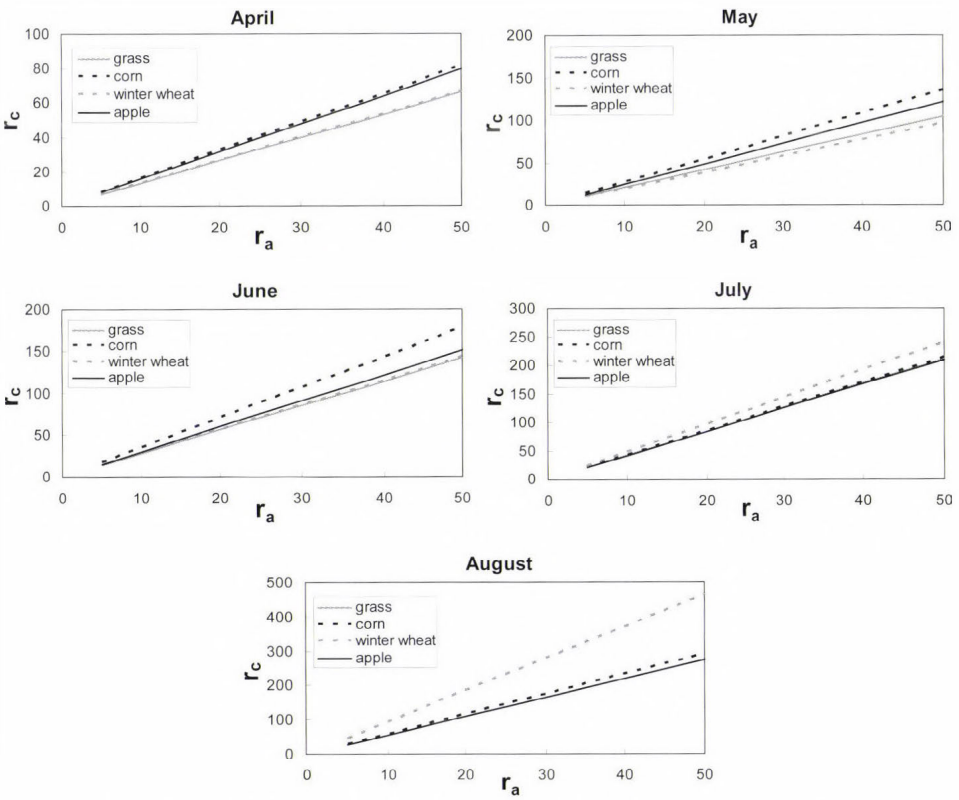

Fig. 3. Dependence between the surface resistance of the land-surface and the aerodynamic resistance for different plant species and months (for the period of April–August).

Note that r_a is estimated as it was described in Section 3, while Δ and β_{hun} were calculated from climate, plant coefficient, and soil data. Two basic features can be observed: first, there is a variability according to the plant species; this is easy to observe, for instance, in May and August, and second, by decreasing r_a values, the obtained plant-specific lines converge to each other into a fix and low r_c value. That is, according to this model, r_c is also weakly dependent on r_a, when the turbulent mixing is large. Annual course of r_c for $r_a = 5$ s m^{-1}, when

turbulent mixing is large enough for all vegetation types considered, is presented in *Fig. 4*. Note that r_c reaches its minimum value when β_{hun} has a maximum, and vice versa, r_c has its maximum value when β_{hun} has a minimum. Furthermore, r_c is mainly governed by F_{ma}, that is by the actual soil moisture content. This is in accordance with the results obtained by *Alfieri et al.* (2008). Plant specific variations of r_c could be observed in May, June, August, September, and October. It is obvious that r_c variations induced by changes of F_{ma} are much larger than the ones induced by plant species changes of b at least in the investigated cases. b-induced differences in May and June are smaller than those obtained in August, September, and October. Note that until June the values of r_c are smaller than 40 s m^{-1}. The high values of r_c for winter wheat in the period after its harvest (August, September, October) refer to bare soil conditions (arable land). It has to be said that our results are in agreement with the results obtained by *Szeicz* and *Long* (1969) as well as *Löpmeier* (1983). *Szeicz* and *Long* (1969) used different methods, among them also the method applied by us, and investigated land-surfaces covered by barley crop and tall grasses. *Löpmeier* (1983) applied lysimeter measurements investigating spring wheat and rye crops.

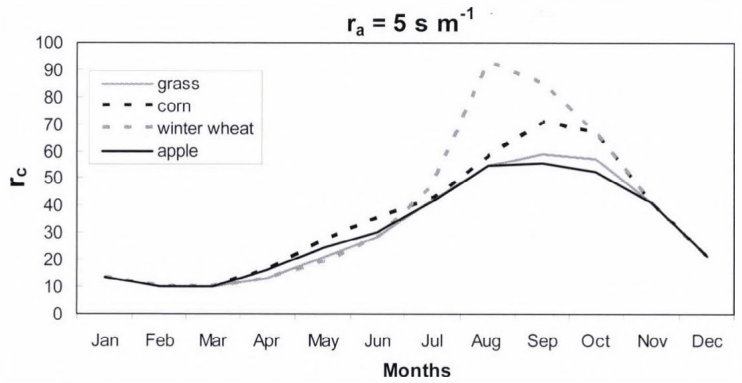

Fig. 4. Annual course of the surface resistance of the land-surface covered by different plant species when $r_a = 5$ s m^{-1}.

4.3. Minimum stomatal resistance values

To estimate r_{stmin}, we shall use the big leaf model of *Jarvis* (1976):

$$r_c = \frac{r_{st\min} \cdot F_{ad}}{LAI \cdot GLF \cdot F_{ma}}, \tag{5}$$

where F_{ad} is the relative stomatal conductance expressing the atmospheric (global radiation, air temperature, and humidity) impact upon stomatal

functioning and *GLF* is the green leaf fraction. Knowing r_c and F_{ma} and making some assumptions for *LAI*, *GLF*, and F_{ad}, r_{stmin} can be inferred. In doing so, first of all, we shall suppose a closed vegetation canopy (this is fulfilled when *LAI* is larger or about 4 $m^2 m^{-2}$), and that *GLF* and F_{ad} equal 1. The latter assumption is quite crude, nevertheless, there are examples in the literature for its use (e.g., *De Ridder* and *Schayes*, 1997). In this case, the stomata are open at a maximum rate (*Ács*, 2008), that is, there is no atmospheric regulation of stomatal functioning. The former assumption that $GLF = 1$ is not rare, this is surely fulfilled at the beginning and in the middle of the growing season. Since direct observations of *LAI* were not available, the course of *LAI* is estimated using Eq. (4). *NDVI* values are taken from *Bartholy et al.* (2004). The LAI_{max} values are chosen after *Masson et al.* (2003). They were 2 and 4 $m^2 m^{-2}$ for tall grass and other vegetation cultures, respectively. These courses of *LAI* for tall grass and other plant species are presented in *Fig. 5*. Since *LAI* is about 4 $m^2 m^{-2}$ only in May and June, r_{stmin} shall be estimated only for these two months.

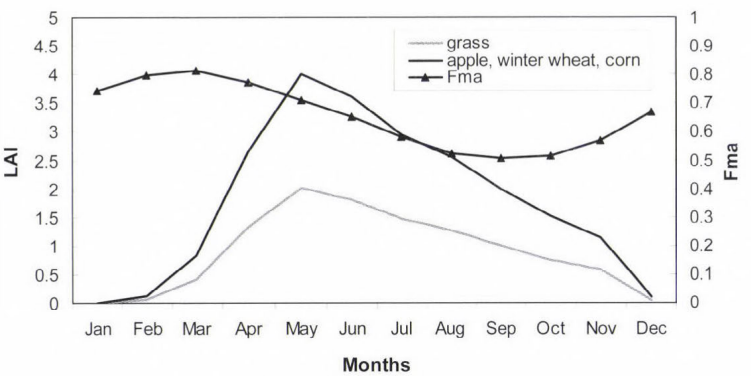

Fig. 5. Seasonal changes of leaf area index for different plant species

The estimated r_{stmin} values for $r_a = 5$ s m^{-1} are presented in *Table 3*. Note that r_c does not depend upon low r_a values. Since r_c and F_{ma} are about equal for both months, r_{stmin} values differ only because of the different *LAI* values. For tall grass r_{stmin} is about 15 s m^{-1}, while for other plant species it is about 35 s m^{-1}. According to *Alfieri et al.* (2008), the r_{stmin} value of grass seems to be too low. They obtained a value of for r_{stmin} about 90 s m^{-1} with a standard deviation of about 40 s m^{-1}. Nevertheless, their grass is wild, while our grass is cultivated. It is well known that r_{stmin} values of the cultivated species are much lower than the r_{stmin} values of the same wild species. r_{stmin} value of 35 s m^{-1} estimated for other plant species is in accordance with the r_{stmin} value obtained by *Alfieri et al.* (2008) referring to croplands. Their suggested r_{stmin} value for croplands is about 20–30 s m^{-1} which is close to our value. It has to be noted that the estimations of *Alfieri et al.* (2008) are based on the field measurements and on the use of the

Jarvis' formula. They also showed that r_{stmin} values are highly changeable in the space and time, which is not a reassuring fact from the point of view of the mesoscale meteorological models which apply Jarvis' formula.

Table 3. Estimated values of canopy vegetation and minimum stomatal resistances for grass and other cultivated vegetation (*other* means the average value of apple, winter wheat, and corn) in the months May and June. F_{ma} indicates the relative stomatal conductance caused by soil moisture deficit and *LAI* is the leaf area index

Month	F_{ma}	r_c		*LAI*		r_{stmin}	
		grass	other	grass	other	grass	other
May	0.71	10.44	11.78	2.0	4.0	14.85	33.53
June	0.65	14.18	15.69	1.8	3.6	16.61	36.76

5. *Conclusions*

In biophysical modeling, the resistance/flux relationship is usually used in a "forward mode" when flux has to be calculated from the known resistance. In contrast to the former case, there is also a "backward mode" calculation when resistance has to be estimated supposing that the flux is known. In this study, a "backward mode" treatment for estimating monthly mean values of crop surface resistance is presented. r_c is calculated estimating the ratio of actual and potential evapotranspiration, β_{hun}, from simulated F_{ma} and observed b values (Eq. 2). r_c is estimated only for small r_a values (strong unstable stratification), when the relationship between the stomata and the near surface atmosphere is strong. In this case r_c is only weakly dependent upon r_a. To the best of our knowledge, this study is the first "backward mode" type study in Hungary in the subject of biophysical modeling.

To apply the method, a set of meteorological, satellite, soil- and vegetation-specific data was used. Meteorological data are taken from CRU, satellite data are obtained from *Bartholy et al.* (2004), location-specific soil data are determined by using the studies of *Nemes* (2003) and *Fodor* and *Rajkai* (2005), while vegetation-specific data are taken from *Posza* and *Stollár* (1983). These latter data are obtained from evapotranspirometer measurements performed at different locations but mostly in Szarvas. The novelty of the analysis does not lie in the methodology applied, but rather in the combination and application of the relevant input data mentioned above. It is shown that r_c is mainly governed by F_{ma}, that is, by the amount of water available for evapotranspiration. It is also shown that r_c variations induced by changes of F_{ma} are much larger than those ones induced by plant species changes represented by b. The results obtained for r_c are in accordance with results published in the scientific literature (e.g., *Szeicz* and *Long*, 1969). We tried to estimate r_{stmin} as well, by using the formula of *Jarvis* (1976) and applying different more or less crude assumptions. The results

obtained in this way are in a quite good agreement with the results obtained by *Alfieri et al.* (2008). This analysis revealed also that r_{stmin} is impossible to estimate without precise knowledge of *LAI*.

The analysis used some "old results" obtained from evapotranspirometer measurements for purposes of biophysical modeling. The opportunity of such an application has been written by *Kozmáné Tóth* and *Hunkár* (1995). The results obtained are instructive in the field of land-surface/atmosphere interaction modeling.

Acknowledgements—This work was motivated by the inspiration that we got by investigating evapotranspirometer measurements done by *Emánuel Antal*, *István Posza*, *András Stollár* and others. Thank you for this motivation.

References

Alfieri, J.G., Niyogi, D., Blanken, P.D., Chen, F., LeMone, M., Mitchell, K.E., Ek, M.B. and *Kumar, A.*, 2008: Estimation of the minimum canopy resistance for croplands and grasslands using data from the 2002 international H_2O project. *Mon Weather Rev 136*, 4452-4469.

Antal, E., 1966: Potential evapotranspiration of some agricultural plant species (in Hungarian). *Öntözéses gazdálkodás 4*(1), 69-86.

Antal, E., 1968: Irrigation schedule on the basis of meteorological data (in Hungarian). *CSc Thesis*, Magyar Tudományos Akadémia, Budapest, 147 pp.

Ács, F., 1994: A coupled soil-vegetation scheme: Description, parameters, validation and sensitivity studies. *J Appl Meteorol 33*, 268-284.

Ács, F. and *Hantel, M.*, 1998: The land-surface flux model PROGSURF. *Global Planet Change 19*, 19-34.

Ács, F., 2008: Meteorological modeling of the soil-vegetation system processes. Applications in science and in education (in Hungarian). *ELTE Eötvös Kiadó*, Budapest, 249 pp.

Bartholy, J., Pongrácz, R., Barcza, Z. and *Dezső, Zs.*, 2004: Aspects of urban/rural population migration in the Carpathian basin using satellite imagery. In *Environmental Change and Its Implications for Population Migration* (eds.: *J.D. Uruh, M.S. Krol* and *N. Kliot*). Kluwer Academic Publishers, 289-313.

Breuer, H., 2009: The strength of the coupling between the vegetation and the atmosphere (in Hungarian). *Légkör 54*(3), 8-11.

Clapp, R.B. and *Hornberger, G.M.*, 1978: Empirical equations for some hydraulic properties. *Water Resour Res 14*, 601-604.

Deardorff, J.W., 1977: A parameterization of the ground surface moisture content for use in atmospheric prediction models. *J Appl Meteorol 16*, 1182-1185.

Deardorff, J.W., 1978: Efficient prediction of ground surface temperature and moisture with inclusion of a layer of vegetation. *J Geophys Res 83*, 1889-1903.

De Ridder, K. and *Schayes, G.*, 1997: The IAGL Land Surface Model. *J Appl Meteorol 36*, 167-183.

Fodor, N. and *Rajkai, K.*, 2005: Estimation of physical soil properties and their use in models (in Hungarian). *Agrokem Talajtan 54*, 25-40.

Hargreaves, G.H. and *Samani, Z.A.*, 1982: Estimating potential evapotranspiration. *J Irrig Drain E-ASCE 108*, 225-230.

Jarvis, P.G., 1976: The interpretation of the variations in leaf water potential and stomatal conductance found in canopies in the field. *Philos Trans Roy Soc, London Ser. B. 273*, 593-610.

Jarvis, P.G. and *McNaughton, K.G.*, 1986: Stomatal Control of Transpiration: Scaling Up from Leaf to Region. *Adv Ecol Res 15*, 1-49.

Justice, C.O., 1986. Monitoring East African Vegetation using AVHRR data. *Int J Remote Sens 6*, 1335-1372.

Kakas, J., 1960: Annual potential evapotranspiration. Annual water excess. Annual water deficit (in Hungarian). Magyarország Éghajlati Atlasza. *Akadémiai Kiadó*, Budapest.

Kozmáné Tóth, E. and *Hunkár, M.*, 1995: Agrometeorology (in Hungarian). In Fejezetek a magyar meteorológia történetéből 1971-1995 (eds.: *A. Simon* and *T. Tänczer*). Országos Meteorológiai Szolgálat, Budapest, 235-257.

Löpmeier, F.-J., 1983: Agrarmeteorologisches Modell zur Berechnung der aktuellen Verdunstung (AMBAV). *Beiträge zur Agrarmeteorologie 7/83*. Deutscher Wetterdienst, Offenbach.

Masson, V., Champeaux, J-L., Chauvin, F., Meriguet, C., and *Lacaze, R.*, 2003: A global database of land surface parameters at 1-km resolution in meteorological and climate models. *J. Climate 16*, 1261-1282.

Mitchell, T., Carter, T.R., Jones, P., and *Hulme, M.*, 2004: A comprehensive set of high-resolution grids of monthly climate for Europe and the globe: The observed record (1901-2000) and 16 scenarios (2001-2100). *Tyndall Centre Working Paper* 55, 30 p.

Monteith, J.L., 1965: Evaporation and environment. *Proc Symp Soc Exp Biol 19*, 205-234.

Nemes, A., 2003: Multi-scale hydraulic pedotransfer functions for Hungarian soils. *Ph.D. Dissertation*, Wageningen University.

Posza, I. and *Stollár, A.*, 1983: Plant constants evaluated by several years' measurements for the calculation of effective evaporation (in Hungarian). *Időjárás 87*, 170–177.

Szeicz, G. and *Long, I.F.*, 1969: Surface resistance of crop canopies. *Water Resour Res 5*, 622–633.

Szesztay, K., 1958: Estimation of water balance of catchment areas in Hungary. *Időjárás 62*, 313-328.

Thornthwaite, C.W. and *Mather, J.R.*, 1955: The water balance. *Drexel Inst. of Techn., Lab. of Clim. VIII.* No. 1, 1–104, N.J.

Turc, L., 1961: Estimation of irrigation water requirements, potential evapotranspiration: a simple climatic formula evolved up to date. *Annals of Agronomy 12*, 13-49.

Wardley, N.W. and *Curran, P.J.*, 1984: The estimation of green leaf area index from remotely sensed airborne multiespectral scanner data. *Int J Remote Sens 5*, 671-679.

Wiegand, C.L., Richardson, A.J. and *Kanemasu, E.T.*, 1979: Leaf area estimates for wheat from landsat and their implications for evapotranspiration and crop modeling. *Agron J 71*, 336–342.

Zhangsi, Y. and *Williams, T.H.L.*, 1997: Obtaining spatial and temporal vegetation data from landsat MSS and AVHRR/NOAA satellite images for a hydrologic model. *Photogramm Eng Rem S 63*, 69-77.

Várallyay, G., Szűcs, L., Rajkai, K., Zilahy P. and *Murányi, A.*, 1980: Hydro-physical classification and 1:100 000 scale maps of Hungarian soils (in Hungarian). *Agrokem Talajtan 29*, 77-112.

IDŐJÁRÁS

Quarterly Journal of the Hungarian Meteorological Service
Vol. 114, No. 3, July–September 2010, pp. 217–227

Modeling of redline dayglow emission

Vir Singh[1*], A. K. Upadhayaya[2], and M. V. Sunil Krishna[1]

[1]*Department of Physics, Indian Institute of Technology Roorkee*
Roorkee – 247 667, India

[2]*Radio and Atmospheric Sciences Division, National Physical Laboratory,*
New Delhi – 110 012, India

[*]*Corresponding author; E-mail: virphfph@iitr.ernet.in*

(Manuscript received in final form August 8, 2008)

Abstract — The present paper deals with the morphological study of redline dayglow emission. The morphology is obtained from the profiles of redline dayglow emission using the updated Glow model. The Glow model is updated in terms of measured various collisional cross sections and reaction rate coefficients. The volume emission rate is obtained for some specific cases (18.3°S, 99.0°E, at 7:33 a.m. on February 1, 1993, 1.3°N, 139.0°E, at 11:30 a.m. on February 11, 1993, 35.2°S, 197.0°E, at 3:13 p.m. on April 2, 1993, and 52.9°S, 207.0°E, at 3:45 p.m. on April 9, 1993) using updated Glow model, and the results are compared with WINDII measurements. The modeled emission rate is found in good agreement with the WINDII observations at all altitudes except in the peak region where model underestimates the WINDII observations within 25%. The updated Glow model is further used to obtain the morphology of redline emission under equinox conditions (for the months of March and April, 1993) between 50°S and 50°N latitudes. It has been found that this emission shows an asymmetry between the Northern and Southern Hemispheres under equinox conditions. The asymmetry in the thermospheric region is likely due to the changing contributions with altitude of the various sources which are responsible for the production of $O(^1D)$ during daytime. The daytime intensity variation is found quite consistent with the WINDII measurements under equinox conditions.

Key-words: airglow, satellite observations, photochemistry, global emission intensity

1. Introduction

Redline dayglow emission is possibly the most extensively observed emission in the dayglow (*Noxon* and *Johanson*, 1972; *Narayan et al.*, 1989; *Sridharan et al.*, 1992; *Shepherd et al.*, 1993). It has now been well established that the redline dayglow emission shows a peak in upper thermospheric region (200–230 km).

The well-known identified sources of redline dayglow emission are dissociative recombination, photoelectron impact on atomic oxygen, and photodissociation of O_2. However, the contribution of reaction of $N(^2D)$ with O_2 to the redline emission in airglow is still a matter of discussion (*Torr et al.*, 1981; *Link*, 1982; *Singh et al.*, 1996; *Link* and *Cogger*, 1988). Although, the altitude range of the production of $O(^1D)$ state extends from 100 to 300 km, the emission is mainly observed above 120 km, as below 120 km the $O(^1D)$ atoms are quenched by molecular nitrogen and molecular oxygen. A number of model calculations (*Hays et al.*, 1978; *Torr et al.*, 1981; *Bates*, 1990; *Singh et al.*, 1996; *Wittase et al.*, 1999) have been carried out to obtain volume emission rates (VER) of redline dayglow emission. These studies have only discussed the volume emission rate profile of 6300 Å in dayglow emission in the light of above mentioned production sources. From these studies one cannot have the idea about the global distribution of redline emission. The wind imaging interferometer (WINDII) has provided numerous data (*Shepherd et al.*, 1993) on redline dayglow emission along with the global distribution between 50°S and 50°N latitudes. WINDII measurements have thus provided an opportunity to study the morphology (volume emission rate as a function of altitude and latitude) of redline dayglow emission using theoretical models. The morphological study of 6300 Å would provide us valuable information about the relative distribution of this emission in both the hemispheres. The most reliable model that has been used to study the airglow emissions is the Glow model developed by *Solomon* (1992). After the development of this model, many input parameters, such as collisional cross-sections, reaction rate coefficients, and quantum yields, have been reexamined experimentally. Consequently the Glow model needs upgrade in light of the newly evaluated parameters.

In the present paper, the morphology of redline dayglow emission is studied in the altitude region of 120 to 300 km under equinox conditions at 10:00 a.m. in local time. The emission profiles are obtained using the Glow model of *Solomon* (1992). The Glow model is updated by using more recent cross-section data, reaction rate coefficients, and variation of solar fluxes. A comparison between the modeled morphology and the observed morphology from the WINDII measurements is made for a specific case for which WINDII data are available. The present morphology is used to discuss the relative variation of 6300 Å dayglow emission in both hemispheres.

2. Model

Mechanisms for the production of redline dayglow emission have been discussed by several workers (*Bates*, 1990; *Link* and *Swaminathan*, 1992; *Tyagi* and *Singh*, 2000), and the following reactions have been identified as the potential sources of redline emission in dayglow:

$$O(^3P) + e_{ph} \rightarrow O(^1D) + e_{ph}, \quad (1)$$

$$O_2^+ + e_{th} \xrightarrow{\eta_D k_2} O(^1S, ^1D, ^3P) + O(^3P), \quad (2)$$

$$N(^2D) + O_2 \xrightarrow{\eta_{2D} k_3} O(^1D) + NO \text{ (not confirmed)}, \quad (3)$$

$$O_2 + h\upsilon \rightarrow O(^1D) + O(^3P), \quad (4)$$

$$O(^1S) \xrightarrow{A_5} O(^1D) + h\upsilon\ (5577\ \text{Å}). \quad (5)$$

In Eqs. (1) and (2), e_{ph} and e_{th} represent photoelectrons and thermal electrons, respectively. A_i and k_i represent the Einstein's coefficient and rate coefficients of the reactions. The production of $O(^1S)$ in Eq. (5) has been discussed by a number of workers (*Tyagi* and *Singh*, 1998; *Singh* and *Upadhayaya*, 2004) in detail. The $O(^1D)$ atoms are quenched by the following reactions:

$$O(^1D) + N_2 \xrightarrow{k_6} O(^3P) + N_2, \quad (6)$$

$$O(^1D) + O_2 \xrightarrow{k_7} O(^3P) + O_2, \quad (7)$$

$$O(^1D) \xrightarrow{A_8} O(^3P) + h\upsilon(6300\ \text{Å}). \quad (8)$$

The Glow model developed by *Solomon* (1992) is used in present calculations, and all the above sources of $O(^1D)$ have been included in the model. The neutral densities and neutral temperature have been used from MSISE-90 neutral atmosphere model (*Hedin*, 1991). The Glow model is updated by using more appropriate O excitation and ionization cross-sections, as given by *Kanik et al.* (1993). The total electron impact cross-section for O is taken as given by *Laher* and *Gilmore* (1990). The transport of photoelectrons and conjugate point effects as given by *Banks* and *Nagy* (1970) and *Nagy* and *Banks* (1970), respectively, have been included in the present calculations. The solar flux values are based on the full F74113 reference solar spectrum of *Hinteregger et al.* (1981), which is scaled using parameterization method based on F10.7 (daily 10.7 cm solar flux) and F10.7A (81 days average of the 10.7 cm solar flux). For ionizing EUV, the bin structure method of *Torr* and *Torr* (1985) is used in the present model. More details about the scaling techniques can be seen in *Upadhayaya* and *Singh* (2002) and *Tyagi* and *Singh* (2000). The total production rate of $O(^1D)$ at an altitude z is given by the following equation:

$$R_z[O(^1D)] = R_{EI}[O(^1D)] + R_{DR}[O(^1D)] + R_{N2D}[O(^1D)] + R_{DS}[O(^1D)] + R_{CAS}[O(^1D)], \quad (9)$$

where R_{EI}, R_{DR}, R_{N2D}, R_{DS}, and R_{CAS} are production rates of $O(^1D)$ due to individual sources for the reactions of Eqs. (1)–(5). Contributions for these individual sources have been discussed in more detail by *Tyagi* and *Singh* (2000). The volume emission rate of $O(^1D)$ at a particular altitude z is given by

$$V_z[O(^1D)] = Q_D R_z [O(^1D)], \quad (10)$$

Q_D is the quenching factor of $O(^1D)$ given by

$$Q_D = \frac{A_8}{A_8 + k_6[N_2] + k_7[O_2]}, \quad (11)$$

where A_8 is the Einstein coefficient for $O(^1D)$ state. The reactions and rate coefficients are given in *Table 1*.

Table 1. Reactions and rate coefficients

Reaction	Rate coefficient ($cm^3 s^{-1}$)	References
$O(^3P) + e_{ph} \rightarrow O(^1D) + e_{ph}$	Impact cross-section	*Laher* and *Gilmore* (1990)
$O_2^+ + e_{th} \rightarrow O(^1D) + O(^3P)$	$k_2 = 1.6 \times 10^{-7}(300/T_e)^{0.5}$	*Walls* and *Dunn* (1974)
$N_2(^2D) + O_2 \rightarrow O(^1D) + NO$	$k_3 = 6.0 \times 10^{-12}$	*Lin* and *Kaufman* (1971)
$O(^1S) \rightarrow O(^1D) + h\upsilon$ (5577 Å)	$A_5 = 1.18\ s^{-1}$	*Nicolaides et al.* (1971)
$O(^1D) + N_2 \rightarrow O(^3P) + N_2$	$k_6 = 3 \times 10^{-11}$	*Hays et al.* (1978)
$O(^1D) + O_2 \rightarrow O(^3P) + O_2$	$k_7 = 2.9 \times 10^{-11}\exp(67.5/T_n)$	*Streit et al.* (1976)
$O(^1D) \rightarrow O(^3P) + h\upsilon$ (6300 Å)	$A_8 = 9.1 \times 10^{-3}\ s^{-1}$	*Nicolaides et al.* (1971)

3. *Results and discussion*

The 6300 Å dayglow volume emission rate profiles are obtained using the updated Glow model for several cases. However, to validate the model results, four cases are shown in *Fig. 1*. *Fig. 1a* shows the results for February 1, 1993 (35.2°S, 197.0°E, at 3:13 p.m., F10.7 = 125.1), *Fig. 1b* shows the results for February 11, 1993 (1.3°N, 139.0°E, at 11:30 a.m., F10.7 = 173.2), *Fig. 1c* shows the results for April 2, 1993 (18.3°S, 99.0°E, at 7:33 a.m., F10.7 = 120.8), and *Fig. 1d* shows the results for April 9, 1993 (52.9°S, 207.0°E, at 3:45 p.m., F10.7 = 135.5). WINDII data are available for these cases. It is quite clear from the values of F10.7 that these cases are for active days.

It is noticeable from *Fig. 1*, that the modeled results are in good agreement with the WINDII measurements except in the peak region, where the model underestimates the WINDII observations within 25%. Calculations have been performed for several other cases as well, and similar agreement is found with the WINDII observations. *Culot et al.* (2004) have also studied the redline emission using the TRANSCAR model and have compared their results with the WINDII observations. The TRANSCAR model also underestimates the WINDII observations, when the solar zenith angle (SZA) is less than 40°. The two cases for February 1, 1993 (*Fig. 1a*) and February 11, 1993 (*Fig. 1b*) have SZA less than 40°, where the model underestimates the WINDII observations within 25%. The other two cases for April 2, 1993 (*Fig. 1c*) and April 9, 1993 (*Fig. 1d*) have SZA greater than 40°, where the model is in very good agreement with the WINDII observations.

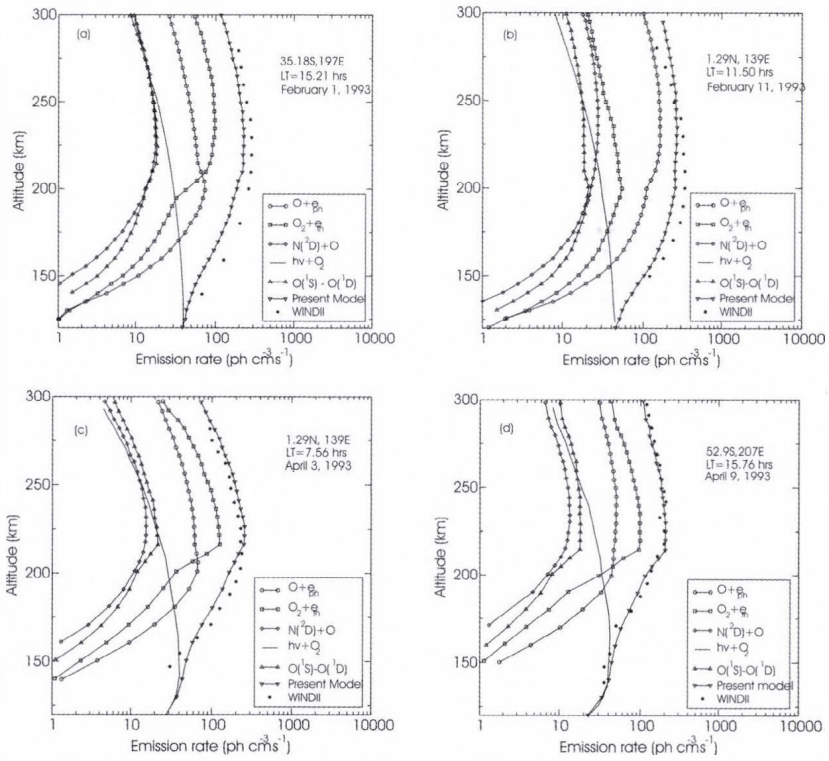

Fig. 1. Modeled and measured redline dayglow emission profiles for selected observing (WINDII) conditions with the various contributions of O(^{1}D) production processes.

The Glow model and the TRANSCAR model are thus quite consistent with each other. Volume emission rates of redline dayglow emission at various latitudes have been calculated along the track of satellite to obtain the

morphology of this emission on February 11, 1993, for which WINDII data are available. On February 11, 1993 the WINDII started measurements of redline emission at 40°S, 2:07 UTC and ended the measurements at 50°N, 2:56 UTC. These observations are shown in *Fig. 2a*. It is quite evident from *Fig. 2a* that the WINDII observations show an asymmetry between the Northern and Southern Hemispheres for redline emission. The modeled morphology of redline emission for this case is shown in *Fig. 2b*. One can notice from *Fig. 2b* that the modeled morphology also shows the asymmetry between the Northern and Southern Hemispheres for the redline emission. It is relatively higher in the Northern Hemisphere than in the Southern Hemisphere between the 30° and 40° latitudes. *Fig. 2c* shows the percentage difference ((Glow model – WINDII / WINDII) × 100) between the modeled results and the WINDII observations for volume emission rate as a function of altitude and latitude for the above case. A close examination of *Fig. 2c* reveals that the modeled results are within 25% agreement with the WINDII observations in the altitude region of 180–220 km. At other altitudes the percentage difference between modeled and WINDII observation is very narrow (much smaller than 25 percent). Consequently, on the basis of the results shown in *Fig. 2c*, one may consider that the model is in good agreement with the WINDII observations.

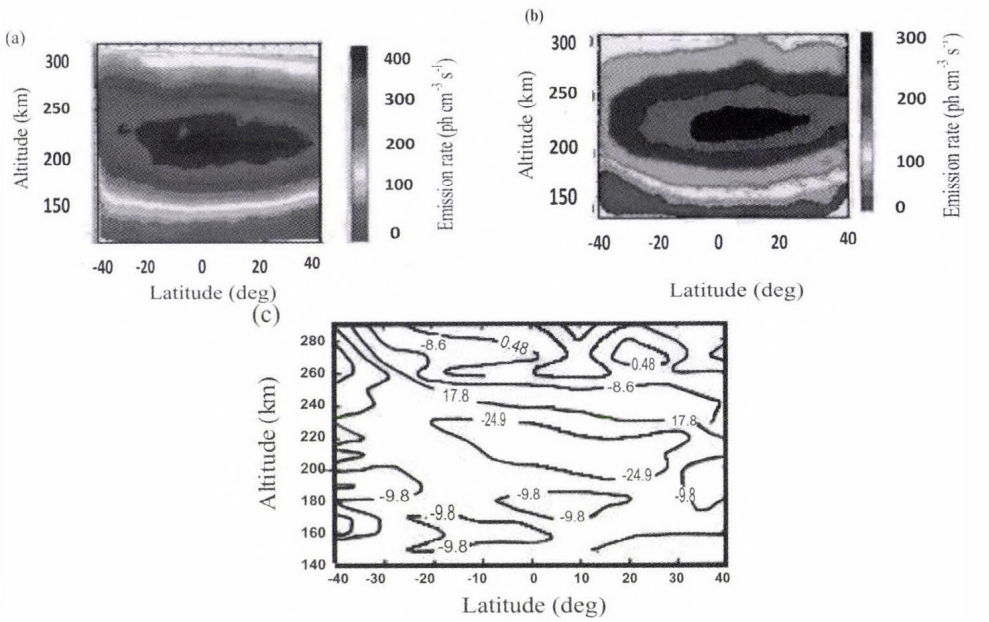

Fig. 2. (a) The altitude/latitude variation of volume emission rates as obtained from WINDII observations on February 11, 1993 (by courtesy of *G.G. Shepherd*). (b) The altitude/latitude variation of volume emission rates as obtained from model on February 11, 1993. (c) The percentage difference (((Glow model – WINDII)/WINDII) × 100) between the model calculations and WINDII observations on February 11, 1993.

The asymmetry of 6300 Å dayglow emission in both hemispheres can be best solved by studying the redline dayglow emission under equinox conditions (for the months of March and April). The reason to choose equinox case is that the sun is closer to the equator (approximate declination of 3°N). Note that this asymmetry in the illumination of the hemispheres due to the present location of the sun does not show any appreciable change (less than 3 percent) over the volume emission rates of redline dayglow emission obtained from the model in both hemispheres under the zero degree declination condition. Consequently, we may use this situation to identify the asymmetry of redline dayglow emission in both hemispheres. The 6300 Å dayglow volume emission rate profiles are obtained at various latitudes between 50°S and 50°N using the Glow model under equinox conditions. The volume emission rate profiles are obtained every fifth day starting from March 1, 1993 to April 30, 1993 at an interval of 5° latitude starting from 50°N, through the equator to 50°S at 10:00 a.m. using the Glow model. Averaging of volume emission rate is done for the above mentioned days for two months (March and April) at various altitudes for a fixed latitude. It would be worthwhile to mention here that the majority of the days during March and April 1993 were having the value of daily F10.7 solar flux greater than 110.

Fig. 3a shows the morphology of redline dayglow emission for 10:00 a.m. A close examination of the contours in *Fig. 3a* reveals that there is a clear asymmetry between the Northern and Southern Hemispheres in the thermospheric peak region (200–240 km) between the 20° and 50° latitudes. This asymmetry is clearly depicted in *Fig. 3b*, where the ratio of Northern to Southern Hemisphere volume emission rates is plotted as a function of altitude and latitudes. It is quite evident from *Fig. 3b* that the redline emission is about 15–20% higher in the Northern Hemisphere in comparison to the Southern Hemisphere between the 30° and 50° latitudes in the thermospheric peak region (200–240 km). The processes of dissociative recombination and photoelectron excitation of atomic oxygen are the dominating sources of this emission in this altitude region, and this, in, turn implies that the dissociative recombination and photoelectron excitation processes seem to be contributing more to redline emission in the Northern Hemisphere in comparison to the Southern Hemisphere. However, one can notice from *Fig. 1* that the contribution to redline emission due to dissociative recombination dominates over the photoelectron excitation contribution at midlatitudes. The TRANSCAR model (*Culot et al.*, 2004) also shows that the relative contribution due to the dissociative recombination process dominates over the photoelectron excitation contribution at midlatitudes. The production rate of $O(^1D)$ atoms due to the dissociative recombination process is proportional to the product of O_2^+ and thermal electron densities. Since, dissociative recombination process is the dominating source at midlatitudes, the asymmetry in redline emission may possibly be attributed due to higher densities of O_2^+ or thermal electrons in the

Northern Hemisphere in comparison to the Southern Hemisphere. However, this fact can only be ascertained if the simultaneous measurements of O_2^+ and thermal electron densities are available in both the hemispheres. It will be worthwhile to mention here, that the transport of photoelectrons is not symmetric about the geographic equator, because photoelectron fluxes are paired by conjugate points, which are not symmetric about geographic equator. Due to this fact, the production of redline emission due to photoelectron excitation process may vary from one hemisphere to another. This asymmetry may be a function of longitude. The results may vary from longitude to longitude. However, this longitudinal variation is not very prominent (the variation is within 5%) and has no strong bearing on the asymmetry of redline emission.

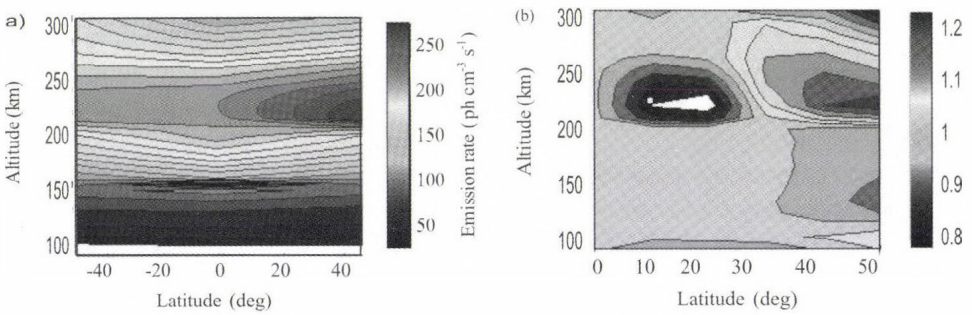

Fig. 3. (a) The altitude/latitude variation of two monthly (March–April 1993) averaged volume emission rates as obtained from model at 10:00 a.m. (b) The ratio of volume emission rate of the Northern to Southern Hemisphere as obtained from the model at 10:00 a.m.

There is no noticeable variation in the ratio of volume emission rates in the lower altitude region (120–180 km). In this altitude region, the photodissociation of O_2 is the dominating source of the production of $O(^1D)$ atoms. It indicates that the contribution to $O(^1D)$ by photodissociation process is more or less uniform in both hemispheres. In *Fig. 4*, the averaged latitudinal variation of intensity for redline dayglow emission is shown under equinox conditions at various local times. The intensities are obtained by integrating the volume emission rate over the vertical column of the altitude for every fifth day starting from March 1, 1993 to April 30, 1993 at an interval of 5° latitude starting from 50°N, through the equator, to 50°S at 8:00, 10:00, 12:00 a.m., 14:00 and 16:00 p.m. in local time. The averaging of intensities is done for the above mentioned days for two months (March and April) at various latitudes. The intensity reaches its maximum at noon, its magnitudes are quite similar at 10:00 a.m. and 2:00 p.m., and it obtaines relatively lower values at 8:00 a.m. and 4:00 p.m.

A variation in intensity from 1.6 KR to 2.1 KR depending on latitude and local time is seen for redline dayglow emissions. This is quite consistent with WINDII measurements as reported by *Zhang* and *Shepherd* (2004).

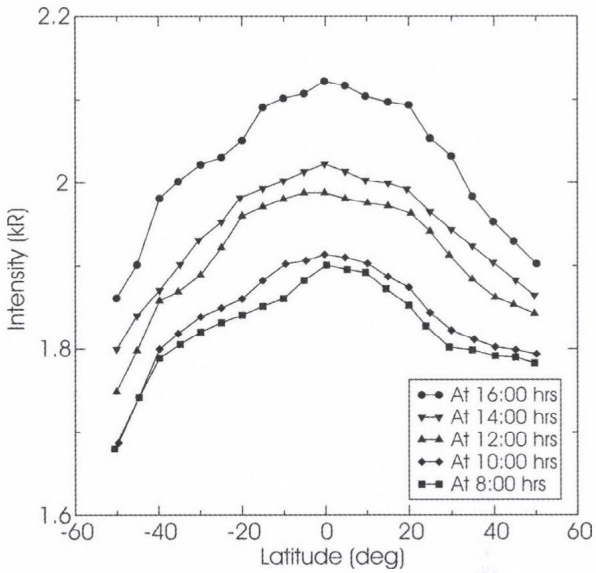

Fig. 4. Averaged latitudinal variation of intensity of 6300 Å dayglow emission under equinox conditions (March–April 1993) at various local times as obtained from the Glow model.

4. Conclusions

The morphology of redline dayglow emission has been studied using the updated Glow model between the 50°S and 50°N latitudes under equinox conditions (for the months of March and April 1993). It has been found that this emission shows an asymmetry between the Northern and Southern Hemispheres. It may be concluded that the asymmetry in the upper thermospheric region is likely due to the changing contributions of the dissociative recombination and photoelectron excitation processes with altitude and latitude. However, the dissociative recombination process seems to be more accountable for the asymmetry found in redline dayglow emission. The present study also indicates that the contribution to $O(^1D)$ by photodissociation process is more or less uniform in both hemispheres. A variation of 1.6 KR to 2.1 KR in intensity depending on latitude and local time is found for this emission, which is quite consistent with the WINDII observations.

Acknowledgement—The authors thank *Prof. G.G. Shepherd*, York University Canada for providing the WINDII data.

References

Banks, P.M. and *Nagy, A.F.*, 1970: Concering the influence of elastic scattering upon Photoelectron transport and escape. *J Geophys Res 75*, 1902-1910.

Bates, D.R., 1990: Oxygen green and redline emission and O_2^+dissociative recombination. *Planet Space Sci 38*, 889-902

Culot, F., Lathuillere, C. and *Lilensten, J.*, 2004: The OI 630.0 and 557.7 nm dayglow measured by WINDII and modeled by TRANSCAR. *Ann Geophys 22*, 1947-1960.

Hays, P.B., 1978: The OI(6300) airglow. *Rev Geophys Space Phys 16*, 225-232.

Hedin, A.E., 1991: Extension of the MSIS thermosphere model into the middle and lower atmosphere. *J Geophys Res 96*, 1159-1172.

Hinteregger, H., Fukui, K. and *Gilson, B.R.*, 1981: Observational references and model data on solar EUV, from measurements on AE-E. *Geophys Res Lett 8*, 1147-1150.

Kanik, K., Trajmar, S. and *Nickel, J.C.*, 1993: Total electron scattering and electronic state excitations cross sections for O_2, CO and CH_4. *J Geophys Res 98*, 7447-7460.

Laher, R.R. and *Gilmore, F.R.*, 1990: Updated excitation and ionization cross sections for electron impact on atomic oxygen. *J Phys Chem Ref Data 19*, 227-305.

Lin, C.-L. and *Kaufman, F.*, 1971: Reactions of metastable nitrogen atoms. *J Chem Phys 55*, 3760-3771.

Link, R., 1982: Dayside magnetosphere cleft auroral processes. *Ph.D. Thesis*, York University, Canada.

Link, R. and *Cogger, L.L.*, 1988: A reexamination of the OI 6300 nightglow. *J Geophys Res 93*, 9883-9892.

Link, R.J. and *Swaminathan, P.K.*, 1992: $N(^2D) + O_2$: A source of thermospheric 6300 Å emission. *Planet Space Sci 40*, 699-705.

Nagy, A.F. and *Banks, P.M.*, 1970: Photoelectron fluxes in the ionosphere. *J Geophys Res 75*, 6261-6270.

Narayanan, R. Desai, J.N. Modi, N.K. Raghavarao, R. and *Sridharan, R.*, 1989: Dayglow photometry: A new approach. *Appl Opt 28*, 2138-2142.

Nicolaides, C. Sinanoglu, O. and *Westhouse, P.*, 1971: Theory of atomic structure including electron correlation. IV. Method for forbidden transition probabilities with results for [OI], [OII], [OIII], [NI], [NII] and [CI]. *Phys Rev A4*, 1400-1410.

Noxon, J.F. and *Johanson, A.E.*, 1972: Changes in thermospheric molecular oxygen abundance inferred from twilight 6300 Å airglow. *Planet Space Sci 20*, 2125-2151.

Shepherd, G.G. et al., 1993: WINDII, the wind imaging interferometer on the upper atmosphere research satellite. *J Geophys Res 98*, 10725-10750.

Singh, V. and *Upadhayaya, A.K.*, 2004: Greenline dayglow emission under equinox conditions. *J Geophys Res 109*, A01308.

Singh, V., McDade, I.C., Shepherd, G.G., Solheim, B.H. and *Ward, W.E.*, 1996: The $O(^1D)$ dayglow emissions as observed by the WIND imaging interferometer on the UARS. *Adv Space Res 17*, 11-14.

Solomon, S., 1992: *Glow Model Version 0.95*. LASP, University of Colorado, Boulder, USA.

Sridharan, R., Haider, S.A., Gurubaran, S., Sekar, R. and *Narayanan, R.*, 1992: OI 630.0nm dayglow in the region of equatorial ionization anomaly: Temporal variability and its causative mechanism. *J Geophys Res 97*, 13715-13721.

Streit, G.E., Carleton, J.H., Schmeltekopf, A.L., Davidson, J.A. and *Schiff, H.I.*, 1976: Temperature dependence of $O(^1D)$ rate constants for reactions with O_2, N_2, CO_2,O_3 and H_2O. *J Chem Phys 65*, 4761-4764.

Torr, M.R. and *Torr, D.G.*, 1985: Ionization frequencies for solar cycle 21: revised. *J Geophys Res 90*, 6675-6678.

Torr, D.G., Richards, P.G., Torr, M.R. and *Abreu, V.J.*, 1981: Further quantification of the sources and sinks of thermosphere $O(^1D)$ atoms. *Planet Space Sci 29*, 595-600.

Tyagi, S. and *Singh, V.*, 1998: The morphology of oxygen greenline dayglow emission. *Ann Geophys 16*, 1599-1606.

Tyagi, S. and *Singh, V.*, 2000: Re-examination of reaction of $N(^2D)$ with O_2 as a source of $O(^1D)$ in dayglow emission. *Indian J Radio Space Phys 29*, 291-295.

Upadhayaya, A.K. and *Singh, V.*, 2002: Effects of temperature dependence of reaction $N_2(A^3\Sigma_u^+)$ + O on greenline dayglow emission. *Ann Geophys 20*, 2039-2045.

Walls, F.L. and *Dunn, G.H.*, 1974: Measurement of total cross sections for electron recombination with NO^+ and O_2^+ using ion storage techniques. *J Geophys Res 79*, 1911-1915.

Wittase, O., Lilensten, J., Lathuilliere, C. and *Blelly, P.L.*, 1999: Modeling the OI 630.0 and 557.7 nm thermospheric dayglow during EISCAT-WINDII coordinated measurements. *J Geophys Res 104*, 24.639-24.656.

Zhang, S.P. and *Shepherd, G.G.*, 2004: Solar influence on $O(^1D)$ dayglow emission rate: Global -scale measurement by WINDII on UARS. *Geophys Res Lett 31*, L07804.

IDŐJÁRÁS

Quarterly Journal of the Hungarian Meteorological Service
Vol. 114, No. 3, July–September 2010, pp. 229–234

Short communication

The virial theorem and planetary atmospheres

Viktor T. Toth

Ottawa, Ontario K1N 9H5, Canada; E-mail: vttoth@vttoth.com

(Manuscript received in final form February 19, 2010)

Abstract—We derive a version of the virial theorem that is applicable to diatomic planetary atmospheres that are in approximate thermal equilibrium at moderate temperatures and pressures and are sufficiently thin such that the gravitational acceleration can be considered constant. We contrast a pedagogically inclined theoretical presentation with the actual measured properties of air.

Key-words: atmosphere, degrees of freedom, hydrostatic equilibrium, thermodynamics, virial theorem

In his widely discussed article, *Miskolczi* (2007) postulates that the virial theorem, which relates the average kinetic and average potential energies of a bound mechanical system (see *Landau* and *Lifshitz* (1972) for a thorough introduction), can be applied to a planetary atmosphere in equilibrium in the planet's gravitational field.

To investigate if Miskolczi's postulate is correct (whether or not the postulate was correctly applied is a question beyond the scope of the present paper), let us first consider the case of a bouncing ball in a homogeneous gravitational field. (The gravitational field within the Earth's atmosphere, the thickness of which is small compared to the Earth's radius, is approximately homogeneous. However, the same results presented here could also be obtained using a Newtonian gravitational potential (*Pacheco* and *Sañudo*, 2003).)

Consider dropping the ball from a height h_b above the surface, and assume that it falls without air resistance, and bounces back from the ground with no loss of kinetic energy. We wish to calculate its average kinetic and average potential energy. It is sufficient to compute these averages for the first part of the ball's motion, as it falls to the ground; the bounce-back is just a time-reversed copy of its initial drop, and afterwards, in the absence of dissipative losses, the ball repeats the same motion *ad infinitum*.

We presume that the ball was dropped at $t = 0$. At any other time $t > 0$, before the ball hits the ground, its height will be

$$h = h_b - \frac{1}{2} g t^2, \tag{1}$$

where g (≈ 9.81 m/s^2 on the Earth) is the surface gravitational acceleration. From this,

$$t = \sqrt{\frac{2(h_b - h)}{g}}, \tag{2}$$

and notably, the time it takes to reach the ground ($h = 0$) is

$$t_0 = \sqrt{\frac{2h_b}{g}}. \tag{3}$$

The velocity of the ball at time t ($0 \leq t \leq t_0$) is

$$v = gt = \sqrt{2g(h_b - h)}. \tag{4}$$

The kinetic energy K and potential energy U of the ball are calculated the usual way:

$$K = \frac{1}{2} m v^2 = \frac{1}{2} m g^2 t^2, \tag{5}$$

$$U = mgh = mgh_b - \frac{1}{2} m g^2 t^2. \tag{6}$$

According to the virial theorem, for a bound mechanical system with kinetic energy K,

$$2\langle K \rangle = \left\langle \sum_a \mathbf{r}_a \mathbf{F}_a \right\rangle, \tag{7}$$

where the angle brackets denote time averaging and $\mathbf{r}_a$ and $\mathbf{F}_a$ are the position of, and the force acting on, the ath particle that constitutes the system. In the case of a system in which the potential energy is a homogeneous function of degree k of the coordinates, we get

$$2\langle K \rangle = k \langle U \rangle. \tag{8}$$

For Eq. (6), $k = 1$. The time averages of the kinetic energy, Eq. (5), and potential energy, Eq. (6), between $t = 0$ and $t = t_0$ can be calculated as

$$\langle K\rangle=\frac{1}{t_0}\int_0^{t_0} K=\frac{1}{6}mg^2t_0^2=\frac{1}{3}mgh_b, \tag{9}$$

$$\langle U\rangle=\frac{1}{t_0}\int_0^{t_0} U=mgh_b-\frac{1}{3}mgh_b=\frac{2}{3}mgh_b. \tag{10}$$

Hence, $2\langle K\rangle=\langle U\rangle$ and the virial theorem for the potential energy, Eq. (6), appears satisfied. This was made possible, in part, by referencing the height h to ground level; this allowed us to ignore the effects of the ground surface in Eq. (7), because at the ground, $\mathbf{r}_a=0$, as observed also by *Pacheco* and *Sañudo* (2003).

How about a column of atmospheric gas? We assume a column of gas in hydrostatic equilibrium standing over a unit surface area in a homogeneous gravitational field. Its density will be a function of height h above ground:

$$\rho=\rho(h). \tag{11}$$

The pressure at h is equal to the weight of gas situated at heights above h:

$$p(h)=\int_h^{\infty} g\rho(h')dh'. \tag{12}$$

We assume that the gas is in thermal equilibrium (the real atmosphere is not in thermal equilibrium, but that is another story), so its temperature is constant:

$$T=T_0. \tag{13}$$

We also assume that the gas obeys the ideal gas law (this is a valid approximation for air at room temperature and sea level pressure), hence

$$pV=nRT, \tag{14}$$

where V is the volume of n moles of gas, and $R\approx 8.31\ \mathrm{J\,K^{-1}\,mol^{-1}}$ is the ideal gas constant. The mass of n moles of gas is nM_n where M_n (≈ 0.029 kg/mol for air) is the molar mass of the gas; its density is $\rho=nM_n/V$, hence $V=nM_n/\rho$. We can thus rewrite the ideal gas law in the form

$$p=\frac{RT_0}{M_n}\rho. \tag{15}$$

Using this in Eq. (12), we obtain

$$\frac{RT_0}{M_n}\rho=\int_0^{\infty} g\rho(h')dh'-\int_0^{h} g\rho(h')dh', \tag{16}$$

or, in differential form,

$$\frac{RT_0}{gM_n}\frac{d\rho}{dh}=-\rho, \tag{17}$$

which can be solved trivially:

$$-\frac{RT_0}{gM_n}\frac{1}{\rho}d\rho = dh, \tag{18}$$

$$-\frac{RT_0}{gM_n}\log\rho = h + C, \tag{19}$$

or

$$\rho = \rho_0 e^{-gM_n h/RT_0}, \tag{20}$$

which we can also write in the form

$$\rho = \rho_0 e^{-h/h_0}, \tag{21}$$

$$h_0 = \frac{RT_0}{gM_n}. \tag{22}$$

For air at $T_0 = 273$ K, we get

$$h_0 = \frac{8.31\times 273}{9.81\times 0.029} \approx 8\text{km}, \tag{23}$$

which agrees well with the observed properties of the atmosphere.

So what about the virial theorem? Going back to the bouncing ball for a moment, we can immediately spot a potential problem: what if the ball is moving horizontally as well? Indeed, it can move horizontally at an arbitrary velocity, yet its potential energy will be no different, hence the virial theorem fails. We must make sure that we only consider the vertical component of the ball's velocity before the theorem can be considered valid. The velocity of the ball can be written in rectilinear form as $v^2 = v_x^2 + v_y^2 + v_z^2$, but we are only interested in the vertical component. In the specific case when the average velocities in the x, y, and z direction are the same, we get $\langle v_z^2 \rangle = \frac{1}{3}\langle v^2 \rangle$. Accordingly, the virial theorem in this case reads

$$\frac{2}{3}\langle K \rangle = \langle U \rangle. \tag{24}$$

This result can also be obtained using another argument, presented by *Pacheco* and *Sañudo* (2003): rather than allowing the coordinates to remain unbounded in the horizontal plane, we can consider confining the ball to within

a cylinder of unit radius, integrating and time averaging the force acting on the ball as it hits the cylinder walls, in order to obtain the right-hand side of Eq. (7).

An atmosphere, unfortunately, is not made of bouncing balls, however appealing that picture might appear. Air, in particular, is composed mainly of diatomic gases (notably N_2 and O_2), which at room temperature have two rotational degrees of freedom in addition to the three translational degrees of freedom discussed above. (At higher temperatures, vibrational modes also play a role.) The kinetic energy of a column of gas is its internal thermal energy. The principle of equipartition of energy states that internal thermal energy is distributed equally between all degrees of freedom. Therefore, the virial theorem now reads

$$\frac{2}{5}\langle K\rangle=\langle U\rangle. \tag{25}$$

This is our main result, valid for any diatomic atmosphere that obeys the ideal gas law in an homogeneous gravitational field at moderate temperatures.

For a column of gas over a unit surface area, the thermal kinetic energy is

$$K=\int_0^\infty c_V T_0 \rho\, dh=c_V \rho_0 T_0 \int_0^\infty e^{-h/h_0}\, dh=c_V \rho_0 T_0 h_0, \tag{26}$$

where c_V is the specific heat of the atmosphere at constant volume. The potential energy is just the gravitational potential energy:

$$U=\int_0^\infty g\rho h\, dh=g\rho_0 \int_0^\infty h e^{-h/h_0}\, dh=g\rho_0 h_0^2. \tag{27}$$

The ratio of the two is

$$\frac{U}{K}=\frac{gh_0}{c_V T_0}. \tag{28}$$

Using Eq. (22), we obtain

$$\frac{U}{K}=\frac{R}{c_V M_n}. \tag{29}$$

Given Eqs. (25) and (29), we can calculate the specific heat c_V. For air, we obtain

$$c_V=\frac{5R}{2M_n}\approx 716\frac{\mathrm{J}}{\mathrm{K\cdot kg}}, \tag{30}$$

a value that agrees well with the known properties of air ($c_V = 718\ \mathrm{J\ K^{-1}\ kg^{-1}}$).

In this derivation, we assumed that $T = T_0$ is constant. Our result, however, remains valid even when T is not constant, so long as the gas is in "local thermodynamic equilibrium", which ensures that the principle of equipartition remains valid and that thermodynamic quantities, such as temperature or specific heat, remain well-defined. To see this, we first rewrite the condition of hydrostatic equilibrium, Eq. (12), in differential form:

$$dp = -g\rho\, dh. \tag{31}$$

This allows us to write the potential energy of the gas, Eq. (27), as

$$U = \int_0^\infty g\rho h\, dh = -\int_0^\infty h\, dp = -\int_0^\infty h \frac{dp}{dh} dh = \int_0^\infty p\, dh, \tag{32}$$

where the last step was taken by integrating in parts and using $p(\infty) = 0$. On the other hand, the thermal kinetic energy, Eq. (26), can be rewritten as

$$K = c_V \int_0^\infty T\rho\, dh = \frac{c_V M_n}{R} \int_0^\infty p\, dh. \tag{33}$$

The ratio of Eqs. (32) and (33) remains the same constant ratio, Eq. (29), that we obtained in the $T = T_0$ case:

$$\frac{U}{K} = \frac{R}{c_V M_n}, \tag{34}$$

even as T varies with altitude. Therefore, even as we allow T to be a function of h, Eq. (25) remains satisfied.

Hence we were able to demonstrate, without having to invoke concepts such as "hard core" potentials or intramolecular forces, that the virial theorem is indeed applicable to the case of an atmosphere in hydrostatic equilibrium. However, it must be "handled with care": the nature of the atmosphere and the fact that the horizontal (translational) and internal (rotational) degrees of freedom of the gas molecules are unrelated to the gravitational potential cannot be ignored.

References

Landau, L.D. and *Lifshitz, E.M.*, 1972: *Theoretical Physics. Vol. I: Mechanics.* Nauka, Moscow.

Miskolczi, F.M, 2007: Greenhouse effect in semi-transparent planetary atmospheres. *Időjárás 111*, 1-40.

Pacheco, A.F. and *Sañudo, J.*, 2003: The virial theorem and the atmosphere. In *Nuovo Cimento C Geophysics Space Physics C*, *26*, 311-316.

Gabriella Szépszó won the 2010 WMO Research Award for Young Scientists

The Executive Council of the World Meteorological Organization (WMO) annually awards prizes for outstanding contributions in the fields of meteorology, climatology, hydrology, and related sciences. The prizes include the publication award Research Award for Young Scientists. This prize was conferred this year to two young researchers, one of them being *Gabriella Szépszó* of Hungary. Gabriella was awarded for the paper entitled "Transient simulation of the REMO regional climate model and its evaluation over Hungary". The paper was published in 2008 in IDŐJÁRÁS by Gabriella and *András Horányi*.

Gabriella is a gifted young scientist, who has been working for the Numerical Modeling and Climate Dynamics Division of the Hungarian Meteorological Service since graduating from the Eötvös Loránd University of Budapest in 2003. I had the opportunity to assist to the first steps of Gabriella in the field of numerical weather prediction, when she started to work at the Hungarian Meteorological Service. Initially she has worked on ensemble prediction systems, but soon she changed her orientation towards climate modeling. She spent several months at the Max Planck Institute for Meteorology in Hamburg as a visiting scientist, and during this stay she deepened her main scientific interest in the field of regional climate modeling and research. As a continuation of her work in Hamburg, she successfully adapted the REMO regional climate model for the Carpathian Basin, and this version has been serving as a research tool for dynamical climate downscaling for the territory of Hungary. Gabriella, together

with her PhD supervisor and coauthor András Horányi, have been carrying out outstanding research in this area in the recent years and with this prize their work is now recognized internationally.

Gabriella Szépszó has been earlier awarded as Prima Junior in the category of science. This prestigious Hungarian prize was conferred to her in 2007 in recognition of both her scientific talent and the importance of the topic of her interest.

It is the second time that a young Hungarian scientist is recognized by WMO for their outstanding research. This is, however, the first occasion that the award is given to the scientist for a publication in our Quarterly Journal IDŐJÁRÁS, which can also indicate the further improving quality of the journal of the last few years. This fact makes also us, the members of the Editorial Board of IDŐJÁRÁS particularly proud and honored.

I am convinced that this prize is a very promising start of a brilliant scientific career, where more similar scientific recognitions are anticipated in the forthcoming decades. I would like to congratulate Gabriella Szépszó on winning this prestigious award and I wish her a very successful future scientific career.

Gábor Radnóti

INSTRUCTIONS TO AUTHORS OF *IDŐJÁRÁS*

The purpose of the journal is to publish papers in any field of meteorology and atmosphere related scientific areas. These may be

- research papers on new results of scientific investigations,
- critical review articles summarizing the current state of art of a certain topic,
- short contributions dealing with a particular question.

Some issues contain "News" and "Book review", therefore, such contributions are also welcome. The papers must be in American English and should be checked by a native speaker if necessary.

Authors are requested to send their manuscripts to

Editor-in Chief of IDŐJÁRÁS
P.O. Box 39, H-1675 Budapest, Hungary
E-mail: antal.e@met.hu

including all illustrations. MS Word format is preferred in electronic submission. Papers will then be reviewed normally by two independent referees, who remain unidentified for the author(s). The Editor-in-Chief will inform the author(s) whether or not the paper is acceptable for publication, and what modifications, if any, are necessary.

Please, follow the order given below when typing manuscripts.

Title page: should consist of the title, the name(s) of the author(s), their affiliation(s) including full postal and e-mail address(es). In case of more than one author, the corresponding author must be identified.

Abstract: should contain the purpose, the applied data and methods as well as the basic conclusion(s) of the paper.

Key-words: must be included (from 5 to 10) to help to classify the topic.

Text: has to be typed in single spacing on an A4 size paper using 14 pt Times New Roman font if possible. Use of S.I. units are expected, and the use of negative exponent is preferred to fractional sign. Mathematical formulae are expected to be as simple as possible and numbered in parentheses at the right margin.

All publications cited in the text should be presented in the *list of references*, arranged in alphabetical order. For an article: name(s) of author(s) in Italics, year, title of article, name of journal, volume, number (the latter two in Italics) and pages. E.g., *Nathan, K.K.,* 1986: A note on the relationship between photo-synthetically active radiation and cloud amount. *Időjárás 90,* 10-13. For a book: name(s) of author(s), year, title of the book (all in Italics except the year), publisher and place of publication. E.g., *Junge, C.E.,* 1963: *Air Chemistry and Radioactivity.* Academic Press, New York and London. Reference in the text should contain the name(s) of the author(s) in Italics and year of publication. E.g., in the case of one author: *Miller* (1989); in the case of two authors: *Gamov* and *Cleveland* (1973); and if there are more than two authors: *Smith et al.* (1990). If the name of the author cannot be fitted into the text: *(Miller,* 1989); etc. When referring papers published in the same year by the same author, letters a, b, c, etc. should follow the year of publication.

Tables should be marked by Arabic numbers and printed in separate sheets with their numbers and legends given below them. Avoid too lengthy or complicated tables, or tables duplicating results given in other form in the manuscript (e.g., graphs).

Figures should also be marked with Arabic numbers and printed in black and white or color (under special arrangement) in separate sheets with their numbers and captions given below them. JPG, TIF, GIF, BMP or PNG formats should be used for electronic artwork submission.

Reprints: authors receive 30 reprints free of charge. Additional reprints may be ordered at the authors' expense when sending back the proofs to the Editorial Office.

More information for authors is available: antal.e@met.hu

Published by the Hungarian Meteorological Service

Budapest, Hungary

INDEX 26 361

HU ISSN 0324-6329